



Charge balance transition enabled *Janus* hydrogel for robust wet-tissue adhesion and anti-postoperative adhesion

Wan Peng^{a,b}, Youjin Lai^a, Yefeng Jiang^a, Yang Zhang^a, Zilin Kan^a, Chuanchao Dai^b, Jian Shen^a, Pingshen Liu^{a,*}

^a Jiangsu Collaborative Innovation Center of Biomedical Functional Materials, Jiangsu Key Laboratory of Bio-functional Materials, School of Chemistry and Materials Science, Nanjing Normal University, Nanjing, 210023, PR China

^b Department of College of Life Sciences, Nanjing Normal University, 210023, PR China

ABSTRACT

Janus hydrogels have recently emerged as promising bioadhesives for efficient wet-tissue adhesion and anti-postoperative adhesion. However, existing *Janus* hydrogel adhesives normally need varied chemical designs of different layers to achieve asymmetric adhesive/anti-adhesive properties on either side. Here, we present a new strategy to construct an adhesive/anti-adhesive *Janus* hydrogel tissue patch accomplished by switching the charge-balance of the hydrogel layers with similar compositions (anionic carboxyl polymer and cationic ϵ -polylysine, EPL). The bottom layer (AL) is formed under acidic condition (pH 2.85), featuring abundant -COOH and -NH₃⁺ residues, which provide rapid & robust adhesion to diverse wet tissues (up to 100.4 kPa) with high bursting pressure (362.5 mmHg), while the top layer (MLT) is formed under neutral condition, achieving a balanced charge between -COOH/-NH₂ and -COO⁻/-NH₃⁺ groups, which mimic the overall electroneutral structure of zwitterionic materials for efficient anti-postoperative tissue adhesion (up to 6 weeks). Further *in vivo* studies validated that the integrated AL/MLT hydrogel patch is biodegradable (within 10 weeks), exhibits broad-spectrum antibacterial activity (up to 99.8%), and outperforms the commercial fibrin gel in sutureless wound sealing, rat gastric tissue repair, and anti-postoperative adhesion. This strategy may open a new avenue to develop adhesive/anti-adhesive *Janus* bioadhesives for efficient non-invasive internal tissue sealing and promoted wound healing.

1. Introduction

Each year, over 300 million surgical procedures are performed globally for tissue joining, wound sealing, and implantation of medical devices [1]. Among these, hand-sewn suturing remains the predominant method for sealing surgical wounds [2]. However, this time-consuming procedure can cause mechanical damage to tissues, potentially leading to adverse postoperative complications such as blood leakage [3], surgical site infections (SSIs) [4,5], inflammation [6], and pathological tissue adhesion with surrounding organs [7]. Tissue adhesives offer a promising alternative to sutures, providing advantages for minimally invasive operations and ease of application [8,9]. Despite this, most commercially available tissue adhesives (e.g., fibrin gel [10], cyanoacrylate glue [11], and bovine serum albumin/glutaraldehyde glue [12]) face challenges in effective internal wound sealing due to weak wet-tissue adhesion or cytotoxicity [13]. Additionally, commonly reported homogeneous hydrogel bioadhesives pose a high risk of inducing postoperative tissue adhesion because of their indiscriminate adhesion properties [14–26].

Janus hydrogel bioadhesives, which exhibit asymmetric adhesive/anti-adhesive properties on either side, have recently attracted great attention for their potential in sealing internal wounds while minimizing undesired tissue adhesion [27–33]. To date, existing *Janus* hydrogel bioadhesives are typically prepared either by blocking the adhesive functional groups on one side of the adhesive hydrogel with ions/polyelectrolytes (e.g. Fe³⁺ [34], Ca²⁺ [35], and chitooligomer [36]) or by multilayer composite processing to integrate the adhesive hydrogel with an anti-adhesive layer composed of zwitterionic polymers [28,31,32,37,38], polyethylene glycol (PEG) [29], or polyvinyl alcohol (PVA) [27]. However, these multilayer *Janus* bioadhesives typically contain two layers with varied chemical designs to fulfill the adhesive/anti-adhesive properties. The adhesive layer is normally engineered with massive free carboxyl (-COOH) groups, which have been proven to strongly bind with tissues *via* amide reactions or electrostatic interactions, while the anti-adhesive layer is usually constructed through the integration of antifouling polymers, forming an antifouling surface to effectively prevent tissue adhesion [28,31,32,37–39]. To the best of our knowledge, to create an

Peer review under the responsibility of editorial board of Bioactive Materials.

* Corresponding author.

E-mail address: liups@njnu.edu.cn (P. Liu).

<https://doi.org/10.1016/j.bioactmat.2025.06.006>

Received 18 March 2025; Received in revised form 25 May 2025; Accepted 2 June 2025

2452-199X/© 2025 The Authors. Publishing services by Elsevier B.V. on behalf of KeAi Communications Co. Ltd. This is an open access article under the CC BY-NC-ND license (<http://creativecommons.org/licenses/by-nc-nd/4.0/>).

adhesive/anti-adhesive *Janus* bioadhesive accomplished by switching the charge-balance of the hydrogel layers with similar chemical compositions has never been reported.

Zwitterionic materials, which contain both cationic and anionic residues yet remain overall electrically neutral, have demonstrated excellent antifouling properties due to their unique charge-balanced structures [40–43]. Inspired by the charge-balance nature of zwitterionic materials, we hypothesize that a zwitterion-free hydrogel, composed of an anionic carboxyl polymer and a cationic amine polymer, might also exhibit strong resistance to tissue adhesion if the anionic/cationic residues in the polyelectrolyte or hydrogel network achieve electroneutrality. Additionally, considering the impact of pH variation on the anionic/cationic balance [44], it is possible to alter the anionic/cationic balance within the hydrogel network through pH adjustment, thereby retaining free carboxyl or/and amine groups for robust binding with tissues *via* hydrogen bonding and electrostatic interactions [39,45].

To test this hypothesis, a *Janus* tissue patch that combined two hydrogel layers with similar chemical composition (anionic carboxyl polymer and cationic EPL) but formed under different pH conditions (the bottom AL hydrogel was formed at acidic conditions, while the top MLT hydrogel was formed at neutral conditions) was constructed. The chemical structure and composition of anionic carboxyl polymers were characterized. The chemical compositions, surface morphologies, and surface chemical compositions of the AL/MLT *Janus* tissue patch were measured. The mechanical properties and swelling performance of the AL/MLT patch were tested. The adhesive ability to diverse wet tissues, biocompatibility, antibacterial ability, and antioxidant activity of the AL/MLT patch were systematically investigated *in vitro* and *ex vivo*. The biodegradability of the AL/MLT patch was assessed *in vivo*. Furthermore, the wound sealing and anti-postoperative tissue adhesion performance of the AL/MLT patch toward rat gastric defects were evaluated *in vivo*.

2. Materials and experiments

2.1. Materials and reagents

Acrylic acid (AA, 99 %), methacrylic acid (MA, 99 %), ammonium persulfate (APS, ≥ 98 %), and *N*, *N*, *N*, *N*'-tetramethylethylenediamine (TMEDA) were purchased from Aladdin. Tannic acid (TA), ϵ -polylysine hydrochloride (EPL, $M_w < 5000$) was purchased from Macklin. *N*-(Methacryloxy) succinimide (NHSMA) was purchased from Balinway Technology Co., Ltd. 1,1-Diphenyl-2-picrylhydrazyl free radical (DPPH \cdot) was purchased from Tokyo Chemical Industry (Shanghai). All solvents were purchased from Sinopharm Chemical Reagent Co., Ltd. Phosphate-buffered saline (PBS), cell culture medium, and L929 cells were purchased from Adamas. The simulated gastric fluid (SGF) was prepared by dissolving NaCl (2 g) in 1000 ml of deionized water, followed by adjusting the pH to approximately 1.5 with 1 M HCl aqueous solution. The simulated intestine fluid (SIF) was prepared by dissolving potassium phosphate monobasic (10.2 g) in 1 L of deionized water, followed by adjusting the pH to approximately 6.8 with 1 M NaOH aqueous solution. Enhanced Cell Counting Kit-8 (CCK8), and Calcein/PI Cell Viability/Cytotoxicity Assay Kit were purchased from Beyotime Biotechnology. Live/Dead Bacterial Viability Kit was purchased from Thermo Fisher. *Staphylococcus aureus* (*S. aureus*) and *Escherichia coli* (*E. coli*) were provided by the Jiangsu Center for Disease Prevention and Control. Sprague-Dawley (SD) rats were purchased from Beijing Vital River Laboratory Animal Technology Co., Ltd. All animal experiments conducted in this study conformed to the Ethics Committee of Nanjing Normal University and have received approval from the Institutional Animal Care and Use Committee (IACUC-20230914).

2.2. Preparation of AL/MLT patch

The *Janus* AL/MLT tissue patch consists of a wet-adhesive AL

hydrogel patch (the bottom layer) and a non-adhesive MLT hydrogel patch (the top layer). To prepare the AL patch, 0.8 mL of EPL aqueous solution (containing 0.1 g of EPL) was mixed with 0.8 mL of PAMN aqueous solution (containing 0.08 g of PAMN copolymer), yielding the AL hydrogel complex under a low pH condition (pH = 2.85). Following the removal of the liquid supernatant, the hydrogel complex was collected and then dissolved in 400 μ L of a 1:1 (v/v) mixture of methanol and deionized water (pH = 2.85), ultimately yielding a transparent liquid precursor of the AL hydrogel patch.

The MLT hydrogel patch was prepared through the hydration of MLT powders. To prepare the MLT powder, typically, 0.5 g of EPL, 0.4 g of methacrylic acid homopolymer (PMA), and 0.025 g of tannic acid were dissolved in 10 mL of deionized water. The pH value of the mixture was adjusted by dropwise addition of NaOH aqueous solutions (1 M), yielding the MLT hydrogel complex under neutral pH conditions (pH = 7). The hydrogel complex was washed in deionized water, freeze-dried, and ground to obtain the MLT powder.

To prepare the AL/MLT patch, the liquid precursor of the AL patch was deposited in a customized silicone/glass mold at a volume of 100 μ L/cm 2 and dried at 60 $^{\circ}$ C, yielding a transparent AL patch (thickness of 0.11 mm unless otherwise specified). Next, the MLT powders were evenly deposited on the top surface of the AL patch at a density of 20 mg/cm 2 , followed by the addition of deionized water to hydrate the powder. The sample was incubated at 60 $^{\circ}$ C for 5 min with a press, yielding the AL/MLT patch. The AL/MLT patch was sealed and stored at 4 $^{\circ}$ C before use.

The chemical composition of the AL/MLT patch was characterized by Fourier Transform Infrared Spectroscopy (FTIR) and UV–vis spectrophotometer. For the FTIR analysis, AL and MLT powders were used. The AL patch was lyophilized and ground to obtain the AL powder. Typically, dry AL or MLT powder was mixed with anhydrous potassium bromide (KBr) at a 1:100 (w/w) ratio. The mixture was thoroughly ground using an agate mortar and compressed into a transparent pellet for FTIR spectral analysis. For the UV scanning, the AL patch was dissolved in a 1:1 (v/v) mixture of methanol and water (pH 2.85) for subsequent analysis. For the UV scanning of MLT, 4 mg of MLT powder was first dissolved in 1 mL of 1 M NaOH aqueous solution, followed by adding 3 mL of 1 M HCl aqueous solution to the resulting solution for subsequent analysis. The surface elemental compositions of the AL/MLT patch were monitored by X-ray photoelectron spectroscopy (XPS, ThermoFisher). The surface and cross-section morphologies were imaged by the scanning electron microscope (SEM, JEOL, JSM-5610LV).

2.3. Mechanical tests

To test the mechanical properties of the AL patch, the dried AL patch was immersed in PBS at 37 $^{\circ}$ C for 24 h to get swelling equilibrium. The swollen AL patch (length: 20 mm, width: 12 mm, thickness: 0.3 mm) was fixed on a dynamic mechanical analysis (DMA) machine (Jinan Metex Test Technology Co., LTD, CMT6203) for tensile strength test at a constant tensile speed of 50 mm min $^{-1}$.

To test the mechanical property of the MLT hydrogel, 350 mg of MLT powder, deposited in a glass-silicone mold, was hydrated by adding 350 μ L of deionized water to the powder. After incubation at 37 $^{\circ}$ C for 20 min, the resulting MLT hydrogel (length: 25 mm, width: 15 mm, thickness: 1.2 mm) with/without soaking in Dulbecco's modified Eagle medium (DMEM) at 37 $^{\circ}$ C for 24 h was fixed on the DMA machine for tensile strength test at a constant tensile speed of 50 mm min $^{-1}$. A mechanical sensor (100 N load cell) was used to monitor the dynamic force, and the tensile strength was automatically calculated from the stress-strain curves.

To test the mechanical properties of the AL/MLT patch, the AL/MLT patch (length: 25 mm, width: 6 mm, thickness: 0.33 mm) was immersed in PBS at 37 $^{\circ}$ C for 24 h and then fixed on the DMA tester for tensile strength tests at a constant tensile speed of 50 mm min $^{-1}$. The lap-shear test was used to measure the adhesive strength between the AL and MLT

layers, with an overlapped area of 13×8 mm. The adhesion strength (A) was determined by the following equation:

$$A = F_{\max}/S \quad (1)$$

Where F_{\max} is the maximum force during the tensile process and S is the adhesion area.

2.4. Adhesion performance of AL/MLT patch

The short-term adhesive strength of the AL/MLT patch to diverse tissue samples was measured via the lap shear test on the DMA machine with a 100 N load cell. The AL/MLT patch (length: 25 mm, width: 13 mm) was applied to the tissue surface with gentle pressing of 5 kPa at 37 °C for 2 min (adhesion area: 13×8 mm). Polyethylene film (thickness of 0.1 mm) was applied on the tissue and MLT surfaces as a stiff backing using cyanoacrylate glue (Deli). The lap shear tests were conducted with a constant tensile speed of 50 mm min⁻¹. The adhesion strength (A) was determined by equation (1). To test the adhesion stability of the AL/MLT patch in wet environments, the integrated tissue and AL/MLT adhesive were sealed in a plastic bag with 2 mL of PBS (containing 0.01 % (w/v) sodium azide) for 24 h at room temperature for the lap shear strength test.

For the visual observation of the AL/MLT patch adhered to diverse wet tissues, the AL/MLT patch (length: 25 mm, width: 13 mm) was applied to the PBS wetted tissue surface (porcine skin, liver, heart, small intestine, stomach) with a gentle press of 5 kPa for 2 min at 37 °C (adhesion area: 13×8 mm). A polyethylene film (thickness of 0.1 mm) was applied to the tissue surface as a stiff backing using cyanoacrylate glue (Deli). Immediately, the tissue loaded with 200 g of weight was lifted by the AL/MLT patch, and the process was captured by a digital camera.

Typically, it is challenging for surgical sutures to form a fluid-tight sealing with the surrounding tissues. Tissue adhesives, capable of acting as a physical patch, offer great advantages in preventing fluid leakage from tissue penetration defects [23]. For comparing the wound-sealing ability between the AL/MLT patch with that of the commercially available fibrin gel, *in vitro* bursting pressure tests on damaged chicken skins (defect: diameter of 3 mm) were performed according to our previous work [39]. The AL/MLT patch (diameter: 12 mm) was used to seal the tissue defect (diameter of 3 mm) with a gentle press of 5 kPa at 37 °C for 1 min. The fibrin gel was applied to the chicken skin defect following the protocol provided by the manufacturer (Zhejiang Selling Pharmaceutical Technology Co.). Additionally, the wound-sealing ability of the AL/MLT patch to *ex vivo* wet tissues (porcine skin, small intestine, and stomach) was also evaluated by bursting pressure tests. The sealed tissues with/without 24-h immersion in PBS were fixed on the testing devices, and pressure was applied via gradual injection of PBS (with an injection speed of 10 mL/min). The fluctuating pressure on the pressure gauge was recorded by a digital camera, and the maximum pressure before PBS leakage was read from the recorded videos and defined as the bursting pressure. For the *ex vivo* wound-sealing assay, the AL/MLT patch was applied on the surface of *ex vivo* organs (porcine heart, small intestine, and stomach with a 10-mm-long incision) with gentle pressing of 5 kPa at 37 °C for 2 min. To evaluate the wound-sealing stability of the AL/MLT patch, the sealed organs were immersed in PBS for 12 h, followed by a macroscopic view of PBS leakage. For *in vivo* wound-sealing assay, AL/MLT patches were used to seal the damaged rat liver and stomach with gentle pressing for 15 s. The morphology at the tissue-hydrogel interface was observed by SEM after 2-min freezing in liquid nitrogen and 24-h freeze drying.

2.5. Antibacterial assay

The ϵ -polylysine is certified to have high antibacterial activity against broad-spectrum bacteria such as *E. coli* and *S. aureus* by

destroying the cell membrane [46,47]. The bactericidal ability of the AL/MLT patch composed of abundant EPL was tested via both quantitative and qualitative analysis.

The agar plate colony counting assay: The antibacterial activities of the AL/MLT, AL, and MLT samples were quantitatively evaluated by the viable bacterial cell counting method. The samples (diameter of 10 mm) were incubated with 1 mL of bacterial suspension (suspended in PBS, *S. aureus*, *E. coli*: 10^4 CFU mL⁻¹) at 37 °C for 9 h. PBS was set as the control group. The resulting bacterial suspension was diluted and plated for viable colony counts at 37 °C for 16–24 h. The bacterial viability (V) was calculated according to the following equation:

$$B = (C_1/C_0) \times 100 \% \quad (2)$$

Where C_1 and C_0 represent the bacterial colonies in the experimental group and control group, respectively.

For qualitative antibacterial analysis, the bacteria were seeded on the surface of a titanium sheet (1×1 cm) by 4-h co-culture in bacterial suspension (suspended in tryptone soybean broth, *S. aureus*, *E. coli*: 10^5 CFU mL⁻¹), and then incubated with the AL/MLT patch in 1 mL of PBS at 37 °C for 9 h. The bacteria on the titanium sheet surface were stained with LIVE/DEAD® Backlight™ Bacterial Viability Kit (ThermoFisher L7012), and imaged by confocal laser scanning microscope (CLSM, Nikon Axio Imager A2). In addition, the bacteria were fixed with a 4 % glutaraldehyde aqueous solution, dehydrated with graded ethanol, dried in the vacuum, and sprayed with gold for SEM imaging.

2.6. Antioxidant assay

Tannic acid is a representative polyphenolic compound and has been approved by the US Food and Drug Administration (FDA) as a food additive for its good antioxidant abilities [48–50]. Therefore, the MLT hydrogel containing trace TA is expected to have good antioxidant activity.

For the antioxidant ability assay of MLT powder, the DPPH· clearance test was performed according to the published study [48]. Typically, 50 mg of MLT powder was added to 5 mL of DPPH· solution (50 μ M in methanol). The mixture was incubated at 37 °C for 1.5 and 3 h, respectively. After centrifugation at 6000 rpm for 5 min, the supernatant was collected for absorbance measurement at 517 nm using an ultraviolet–visible spectrophotometer. The DPPH· solution with/without ML powder was set as a control group.

The intracellular antioxidant ability of MLT hydrogel was detected by DCFH-DA of the ROS assay kit (Beyotime). The MLT hydrogel (diameter = 10 mm) prepared by adding 40 μ L of PBS into 40 mg of MLT powder (pre-sterilized by UV irradiation) was immersed in 1 mL of high glucose DMEM for extraction medium collection. Human normal hepatocytes L-02 (2.5×10^4 cells) and Raw 264.7 macrophages (5×10^4 cells) suspension were seeded on 48-well plates, respectively. After incubation for 24 h, the culture medium was removed. The hydrogel, together with 360 μ L of extraction medium and 40 μ L of H₂O₂ (1 mM), was added to the well and incubated with cells for 90 min at 37 °C. The cells incubated with/without H₂O₂ (100 μ M in DMEM) were set as the negative and positive control groups, respectively. The ROS production was measured by a fluorescence microscope (Nikon, Ti-S) with DCFH-DA staining.

2.7. In vitro biocompatibility assay

The cytocompatibility of the AL, MLT, and AL/MLT patches was assessed using L929 fibroblast cells according to the published protocol [51]. To prepare the extracted medium for the *in vitro* cytotoxicity test, the AL/MLT patch (diameter of 10 mm, weight of 40 mg) and the AL and MLT patches within the AL/MLT patch were deposited in the well of a 24-well plate, and 1 mL of high glucose DMEM medium was added to each well. The 24-well plate was placed in a cell incubator containing 5

% CO₂ for 24 h. At the predetermined time, 1 mL of DMEM medium was added to each well, and the mixture was filtered with a 0.22- μ m sterile syringe filter to obtain the extracted liquid. Pristine DMEM was set as a control. L929 cells (5×10^3 cells) were seeded in the well of a 96-well plate and cultured for 24 h. The culture medium in each well was replaced with 0.1 mL of extraction medium containing 10 % FBS. After co-incubation for 1, 3, and 5 days, the viability of L929 cells was quantitatively tested by CCK-8 cell viability kit and qualitatively analyzed by Calcein/PI Cell viability/cytotoxicity assay kit. The culture medium was replaced with fresh extracted liquid containing 10 % FBS at 1, 3, and 5 days.

The hemocompatibility of the AL/MLT patch was evaluated via the hemolysis ratio. Typically, red blood cells (RBC) separated from the fresh rat blood were suspended in PBS (2 v/v%). The AL/MLT patch (dry weight of 36 mg) was incubated with 3 mL of diluted RBC suspensions at 37 °C for 1 h. RBC suspended in PBS (2 v/v%) and Triton X-100 (2 v/v%) were set as the negative and positive control groups, respectively. After centrifugation at 3000 rpm for 5 min, the supernatant was collected for absorbance measurement at 540 nm using a UV-vis spectrophotometer. The hemolysis ratio (H) of the AL/MLT patch was calculated according to the equation:

$$H = [(A_E - A_P) / (A_T - A_P)] \times 100 \% \quad (3)$$

Where A_E , A_T , and A_P were the absorbance of the experimental, positive control, and negative control groups, respectively.

2.8. *In vivo* biodegradability assay

To investigate the responsive degradation behavior *in vivo*, the AL/MLT patch (diameter of 8 mm, thickness of 0.2 mm) was implanted subcutaneously according to our previous work [37]. A 2-cm long incision was created on the rat's back skin. The AL/MLT patch with pre-ultraviolet illumination was subcutaneously implanted. After implantation for 2, 6, and 10 weeks, tissues around the sample were collected for H&E staining. Tissue specimens were fixed in 4 % paraformaldehyde for 12 h at 4 °C. After fixation, samples were progressively dehydrated in an ethanol series (70 %, 80 %, 85 %, 90 %, 95 %, and 100 %), cleared in xylene, and then embedded in paraffin wax for sectioning. Serial tissue sections (5–7 μ m thickness) were obtained using a rotary microtome. For H&E histological staining, sections were first dewaxed in xylene for 10 min and rehydrated through a graded ethanol series (100 %, 90 %, 80 %, 70 %) followed by immersion in deionized water. The sections were stained with hematoxylin and eosin dyes following the protocol provided by the manufacturer (Nanjing Jiancheng Technology Co., Ltd.). Finally, stained sections were dehydrated in ethanol, cleared in xylene, and mounted with neutral resin for microscopic observation.

2.9. Sealing and repairing of gastric defects by AL/MLT patch

The sealing ability of the AL/MLT adhesive to gastric perforation was evaluated on the rat stomach. After anesthesia, the rat's abdominal skin was shaved and sterilized, respectively. A 3-cm skin incision was created along the abdominal midline to expose the stomach. Next, a 4-mm perforation was created at the stomach. The AL/MLT adhesive (pre-sterilized by UV irradiation, diameter of 12 mm, thickness of 0.15 mm) was deployed on the surface of the gastric defect with a gentle press for 10 s. Then, the abdominal incision was closed with a non-absorbable 4-0 suture. Suturing and fibrin glue treatments were set as the positive control groups. After the surgery, all rats were kept fasting for 36 h before resuming a normal diet. On day 7 after surgery, gastric tissues at the surgical site were collected and fixed in 4 % paraformaldehyde solution for 12 h for histological analysis.

3. Results and discussion

3.1. Preparation and characterization of AL/MLT patch

To create the adhesive AL gel, an anionic carboxyl copolymer (PAMN), consisting of acrylic acid, methacrylic acid, and N-(methacryloxy) succinimide with a molar ratio of 50:50:4, was synthesized via conventional radical polymerization (Fig. S1a). This copolymer is capable of crosslinking with cationic EPL through -COOH/-NH₂ hydrogen bonding and -COO⁻/-NH₃⁺ electrostatic interactions, thereby forming a physical hydrogel. ¹H NMR analysis confirmed that the actual compositions of the PAMN closely matched the feeding molar ratio (Fig. S1b). Following the simple mixing of PAMN and EPL, the hydrogel complex was dispersed in a mixture of methanol and deionized water and then air-dried, yielding a transparent AL patch (Figs. S2 and S3a). To construct the top MLT hydrogel layer, which has a similar composition containing identical initial functional cationic and anionic groups to that of the AL layer, the anionic carboxyl polymer (PMA) and EPL were mixed under neutralized condition (pH 7.0) with a trace amount of negatively charged tannic acid incorporated as the potential antioxidant reagent (Fig. S4). Upon water absorption, the AL patch transformed into an adhesive AL gel (Fig. S3b). The -COOH/-NH₂ hydrogen bonding and -COO⁻/-NH₃⁺ electrostatic interactions not only facilitated the quick gelation of MLT powder on the top surface of the AL gel but also enabled robust integration of the AL/MLT patch.

To verify the chemical structures and the charge status of the AL and MLT layers, the AL/MLT patch was characterized by FTIR, XPS, and zeta potential tests. FTIR spectra (Fig. 2a) revealed the characteristic peak at 1710 cm⁻¹, attributed to the carboxylic acid groups from the PAMN component of AL. In contrast, the density of the peak significantly decreased in the MLT powder, while a new peak at 1550 cm⁻¹, associated with carboxylate groups, appeared (Fig. 2a). Additionally, N_{1s} high-resolution scan spectra indicated the presence of three nitrogen species in the AL patch: NH_3^+ (401.5 eV), -O=C-NH- (~400 eV), and -NH₂ (399.5 eV), with percentages of 42, 48, and 10 %, respectively (Fig. 2b and c). The contents of amide species (-O=C-NH-) and amino species (-NH₂/-NH₃⁺) were closely aligned with the stoichiometric ratio of nitrogen species in EPL. In contrast, the content of -NH₃⁺ species in MLT powder drastically decreased from 42 to 17 %, while that of -NH₂ species increased from 10 to 36 % (Fig. 2d). To assess the net charge status of AL and MLT layers, zeta potentials were measured under acidic and neutral pH conditions, respectively. Results showed that the zeta potential of AL was +38.6 mV at acidic pH (2.85), while MLT powders exhibited a zeta potential of +0.6 mV at neutral pH (7.0) (Fig. 2e and S5). It has been reported that mixed-charge polyelectrolytes could also exhibit good antifouling ability when the net charge of the polyelectrolyte is neutral [52–54]. This could be attributed to the good charge balance between cationic and anionic groups in the mixed-charge polyelectrolytes, which can mimic the balanced charge structures of zwitterionic materials (well-known antifouling materials) and thus result in significantly inhibited interactions between the polyelectrolytes and surrounding tissues/cells. Therefore, a net neutral charge of the mixed-charge MLT complex could endow good anti-adhesion performance.

These findings indicate that at low pH, below the pK_a of the carboxylic acid, the carboxylic/carboxylate pendants of the PAMN copolymers are predominantly in the nonionic -COOH status, while the amine groups in the EPL polymer exist mainly as the positively charged -NH₃⁺. This -COOH/-NH₃⁺ couple enabled a net positive charge of the AL patch. Conversely, at neutral pH, the PAMN copolymer exhibits a mix of anionic carboxylate and nonionic carboxylic states, while the amine groups in the EPL polymer exist as a combination of nonionic -NH₂ (predominant) and cationic (-NH₃⁺) states, resulting in a balanced charge in the MLT layer. Notably, when the AL powder is placed in neutral pH conditions and the MLT powder in acidic conditions, their zeta potentials turned to be similar to each other in identical conditions (Fig. 2e), indicating the reversibility of charge balance within the AL and MLT

layers in response to pH fluctuations. When the AL patch is placed in a neutral condition (e.g. PBS, pH 7.2), the -COOH group in PAMN copolymers shifts to be the anionic carboxylate state, while the -NH_3^+ in EPL transforms to the nonionic -NH_2 state, resulting in increased physical crosslinking within the AL hydrogel due to the newly formed $\text{COOH}/\text{-NH}_2$ hydrogen bonding and $\text{-COO}^-/\text{-NH}_3^+$ electrostatic interaction, as evidenced by the limited swelling of the AL hydrogel in PBS and its similar failure tensile strength to the neutralized MLT hydrogel (Fig. S6). These data not only verified the feasibility of switching the charge balance of the hydrogel through simple pH adjustment but also demonstrated the generality of adjusting the charge balance of the hydrogel complex with similar chemical structures.

Due to the co-existence of massive $\text{-COOH}/\text{-NH}_2$ and $\text{-COO}^-/\text{-NH}_3^+$ couples in MLT powders, the dynamic intermolecular interactions (hydrogen bonding and electrostatic interaction) between these couples facilitate rapid water absorption and gelation (Fig. 2f and S7), impressive self-healing capability (a net 59.6 % recovery of the tensile stress after 30-min re-contacting at 37 °C, Fig. S8), limited swelling ratio at neutralized condition (less than 100 % in PBS within 16 days 37 °C, pH = 7.2–7.4), and slow dissolution in a highly acid environment (SGF, pH = 1.5, 37 °C, Fig. 2g). In addition, due to the similar components between the AL patch and MLT powders, the MLT powders can quickly gel on the flat surface of the AL patch (110 μm), and integrate effectively (Fig. 2h), as indicated by the high external force (up to 149.9 kPa) required to prevent the separation of the AL and MLT hydrogel layers

(Fig. 2i & S9a). The integrated AL/MLT patch exhibited deformation after 24-h immersion and a limited swelling ratio (less than 100 %) in PBS at 37 °C for 14 days (Fig. S10), withstanding external tensile strength over 200 kPa after 24-h immersion and an elongation rate exceeding 700 % after 24-h immersion in PBS (Fig. 2j & S9b).

3.2. Adhesive/anti-adhesive performance of the AL/MLT patch

To achieve effective and bio-safe wound sealing & healing for internal tissue defects, tissue adhesives should enable robust adhesion to wet tissues, maintaining sufficient mechanical strength throughout the healing process while preventing adhesion to surrounding tissues and organs [55]. Free carboxyl/amine groups on hydrogel surfaces can form hydrogen bonding/electrostatic interactions (Fig. 1b) with tissue surface functional groups (e.g., -COOH and -NH_2), facilitating instant strong adhesion [56]. Given the varied anionic/cationic charge balances in the AL and MLT layers, the adhesive performances of these two layers of the patch were evaluated *in vitro* and *ex vivo*.

The bottom layer of the AL/MLT patch demonstrated a firm adhesion to the wet porcine stomach with a gentle press, while its top layer could be easily peeled off (Fig. 3a), confirming the different adhesion properties of the AL/MLT patch on either side. Further protein adsorption assay showed that the MLT layer in the AL/MLT patch exhibited minimal adsorption to BSA (Fig. S11), indicating the good antifouling ability of the MLT layer by simulating the charge-balance chemical structures of

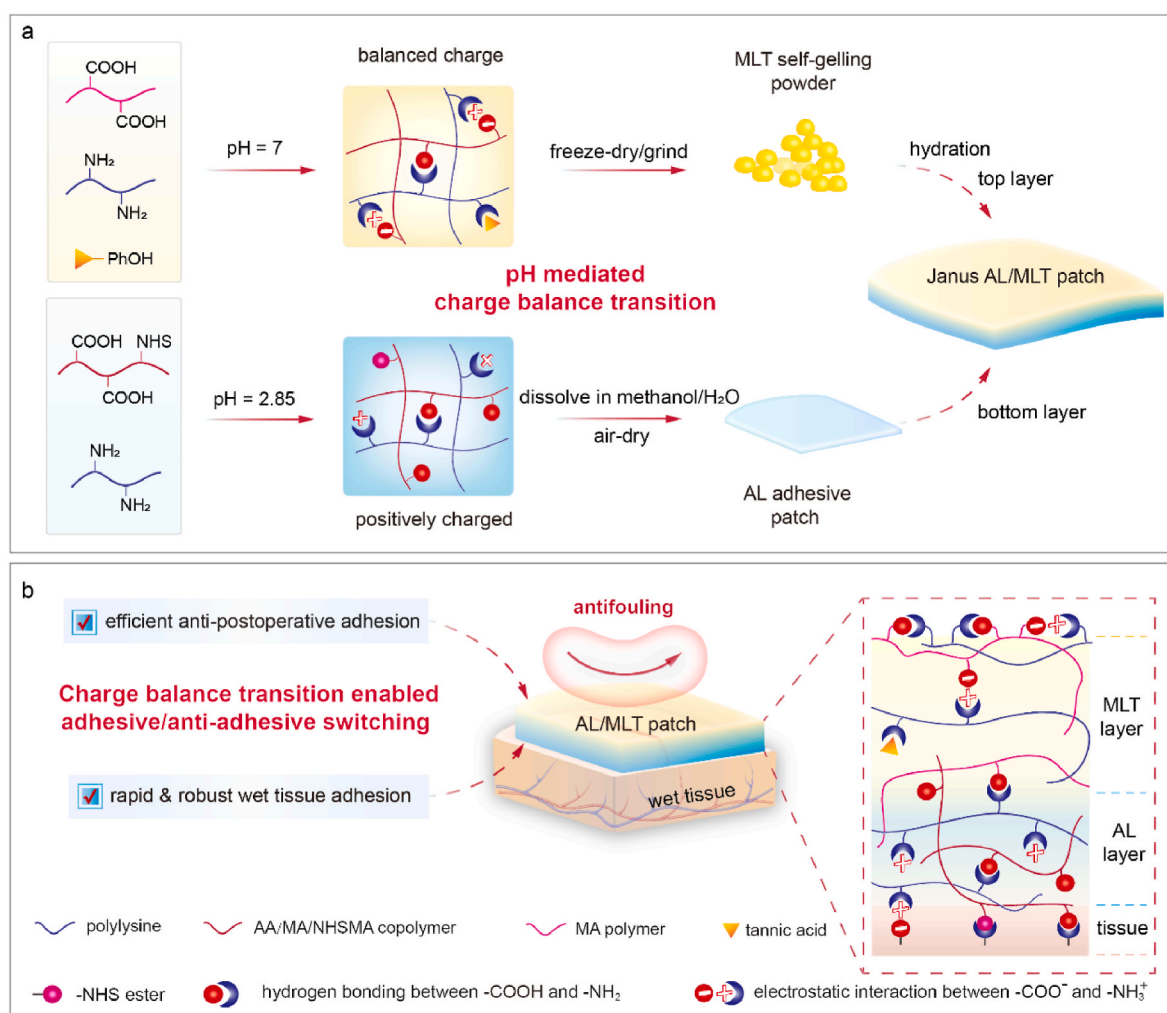


Fig. 1. Design and preparation of the Janus AL/MLT patch. (a) Schematic illustration of the preparation and structure of the Janus AL/MLT patch with varied charge balances enabled by pH adjustment. (b) Schematic illustration of the asymmetric adhesive/anti-adhesive properties enabled by the charge balance transition in the AL/MLT hydrogel patch.

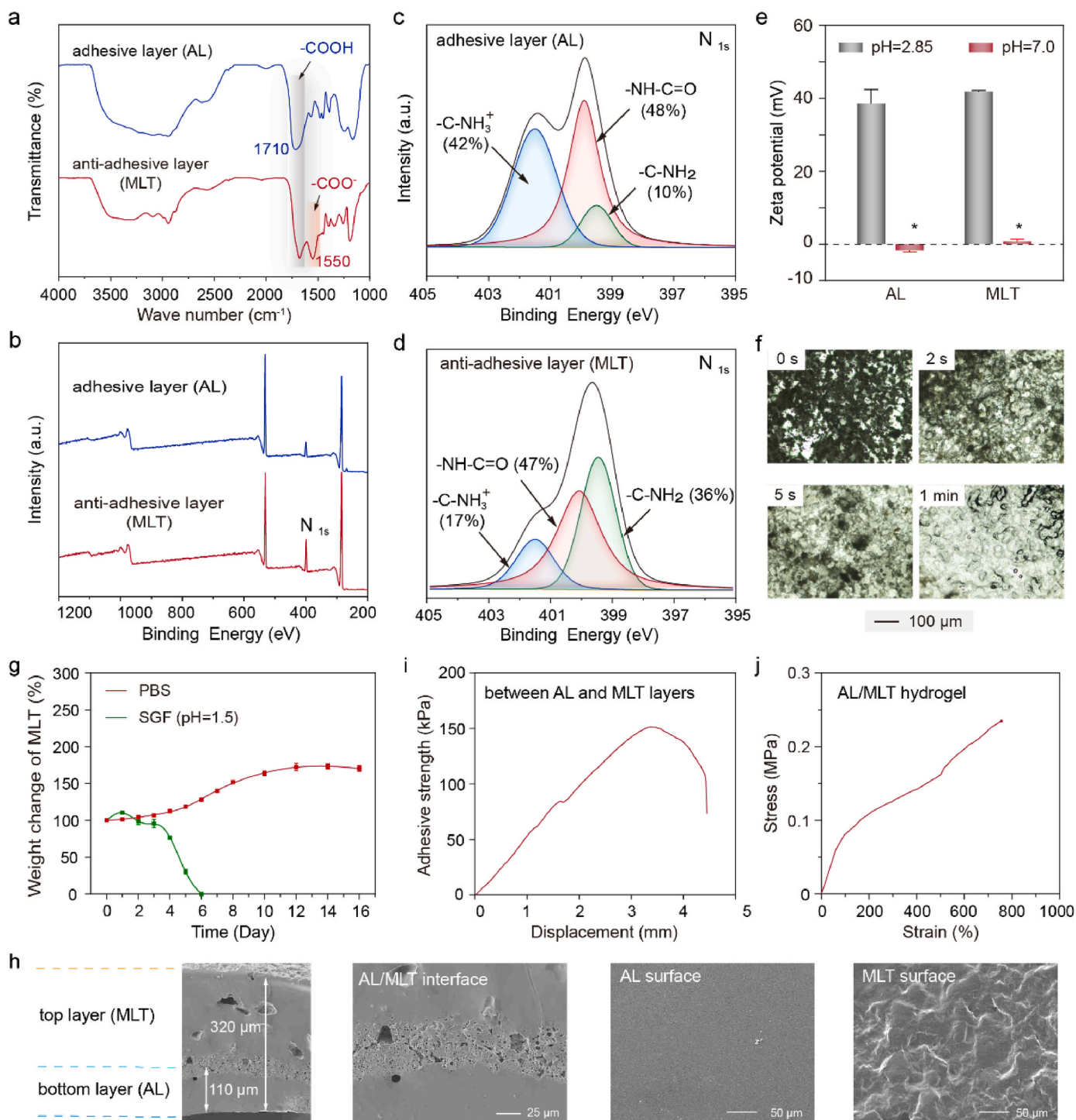


Fig. 2. Characterization of the AL/MLT patch. FTIR spectra of (a) AL and MLT layers. (b) XPS survey scan on the surface of the AL and MLT layers in the AL/MLT patch. High-resolution XPS scan spectra of N_{1s} on the (c) AL and (d) MLT layers. (e) Zeta potentials of the AL and MLT samples, dispersed in deionized water with different pH values. (f) Microscope photos of the gelation process of MLT powders. (g) Swelling performance of the MLT hydrogel in PBS (pH = 7.2) and SGF (pH = 1.5) at 37 °C. (h) SEM images of the AL/MLT patch's cross-section and surface morphologies. (i) Adhesive strength between the AL and MLT layers of the AL/MLT patch. (j) Failure tensile strength versus stretch curve for the AL/MLT patch after 24-h soaking in PBS (pH = 7.2) at 37 °C. Pairwise comparisons of different groups are statistically significant (*, $p < 0.05$) as determined by Student's t-test ($n = 3$).

zwitterionic materials. Visual adhesion demonstrations showed that the AL/MLT patch was capable of adhering to various wet tissues (skin, liver, small intestine, heart, and stomach) through the AL bottom layer, lifting a 200 g weight with an overlapped area of 104 mm² (Fig. 3b). The short-term adhesion strength of the AL/MLT patch to these tissues was 100.4, 46.3, 50.9, 47.9, and 49.9 kPa (Fig. 3c and S12), showcasing

superior wet-adhesive performance to commonly used commercial tissue sealants, including fibrin glue and cyanoacrylate sealant [24]. Notably, after 24-h incubation in PBS, no significant decreases in adhesive strength were observed between AL/MLT patches and diverse tissues (105.1, 42.5, 46.9, 44.53, and 41.5 kPa, Fig. 3c), indicating the robust & stable adhesion capability of the AL/MLT patch to wet tissues.

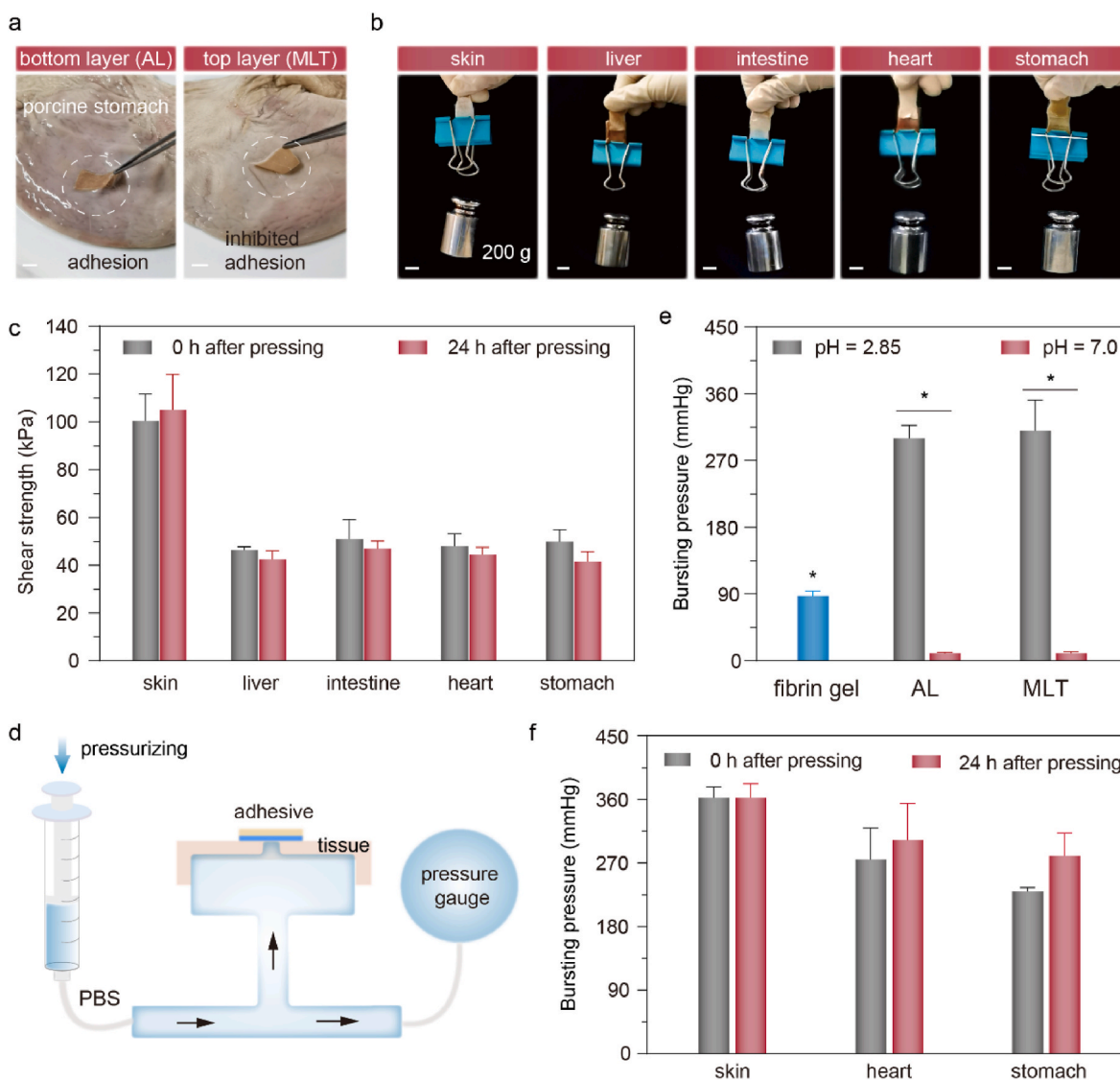


Fig. 3. Adhesion performance of the AL/MLT patch on various tissues. (a) Images of the adhesion performance of the top and the bottom layer to the wet porcine stomach. Scale bar: 10 mm. (b) Images of adhesive performance of AL/MLT patch to porcine skin, liver, small intestine, heart, and stomach. All the adhered construction can lift a weight of 200 g. Scale bar: 4 mm. (c) Adhesion strength of AL/MLT patch on various tissues. (d) Schematic illustration of the bursting pressure test model. (e) Bursting pressures of chicken skin tissues sealed by the fibrin gel, the AL and MLT layers in the AL/MLT patch at pH 2.85 and 7.0. (f) Bursting pressure of porcine skin, heart, and stomach sealed by AL/MLT patch with/without being immersed in PBS (pH = 7.2) at 37 °C for 24 h. Pairwise comparisons are statistically significant (*, $p < 0.05$) as determined by one-way ANOVA multiple comparisons.

In addition to the instant strong adhesion enabled by the hydrogen bonding/electrostatic interactions (Fig. 1b) with tissue-surface functional groups (e.g., -COOH and -NH₂), interfacial covalent bonding provided by the conjugation between the NHS pendants on the AL surface and amine groups on the tissue surface further contributes to the robust adhesion observed (as indicated by Fig. S13).

To achieve effective wound sealing, tissue adhesive is required to resist high pressure from body fluids (e.g., blood, gastrointestinal contents). To evaluate the wound-sealing ability of the AL/MLT patch, a customized model was used to test the burst pressure (Fig. 3d). Results showed that the AL layer in the AL/MLT patch could maintain the sealing status until a burst pressure of 300 mmHg (Fig. 3e). This pressure is significantly higher than that of the commercial fibrin glue (87.5 mmHg). In contrast, a very low burst pressure (10 mmHg) was observed when the MLT side was applied, mainly due to the minimal free -COOH/-NH₂ groups on the MLT surface. Moreover, the addition of a trace amount of tannic acid demonstrated minimal influence on the adhesion performance of the MLT layer (as indicated by Fig. S14). Both

the ML and MLT hydrogels exhibited very low adhesion to wet porcine skin (<2 kPa), regardless of the incorporation of tannic acid. Notably, upon adjusting the pH of the AL layer to 7, the resulting AL layer exhibited a minimal bursting pressure of 10 mmHg (Fig. 3e), as low as that of the MLT layer at neutral pH. This could be attributed to the good charge balance in the overall electrically neutral AL and MLT layers under neutral pH conditions (as evidenced by Fig. 2e). Moreover, this dynamic pH-responsive adhesion/anti-adhesion switching was also observed in the MLT layer. When the neutral MLT powder was placed under acidic pH conditions, the resulting MLT layer (pH 2.85) was able to strongly adhere to the wet tissue surface and maintain a fluid-tight sealing until a bursting pressure of 310 mmHg, comparable to that of the AL layer at pH 2.85.

Further wound sealing performance assays showed that the bursting pressures of the AL layer (pH 2.85) in the AL/MLT patch against the porcine skin, heart, and stomach defects were 362.5, 275, and 230 mmHg, respectively (Fig. 3f), higher than the normal arterial blood pressure (~140 mmHg) and intra-gastric pressure (15–25 mmHg) [57].

After 24-h soaking of the tissue/patch constructs in PBS (pH = 7.2), the bursting pressures were comparable to their original values (362.5 vs. 362.5, 302.5 vs. 275, 280 vs. 230 mmHg), indicating a robust wound-sealing endowed by the AL/MLT patch. *Ex vivo* sealing tests further confirmed the fluid-tight wound sealing ability of the AL/MLT patch to porcine small intestine, heart, and stomach, even after being immersed in excessive PBS for 12 h (Fig. 4a–c). Remarkably, *in vivo* adhesion demonstrations showed that a thin AL/MLT patch could firmly adhere to a rat's liver or stomach within 15 s, effectively preventing leakage of body fluid. SEM imaging on the adhesion interface illustrated the intimate contact and tight bonding between the two substrates as

indicated by the dotted yellow line (Fig. 4d), suggesting that the bottom layer could quickly absorb water from wet tissue surfaces to promote polymer diffusion and adhesion formation. Overall, these findings demonstrated that the AL/MLT patch possesses asymmetric adhesion on either side, enabling rapid & robust wound sealing for internal tissues while effectively preventing undesirable adhesion to adjacent tissues.

3.3. *In vivo* sutureless sealing and healing of gastric defects by the AL/MLT patch

To further test the *in vivo* performance of the AL/MLT patch, a

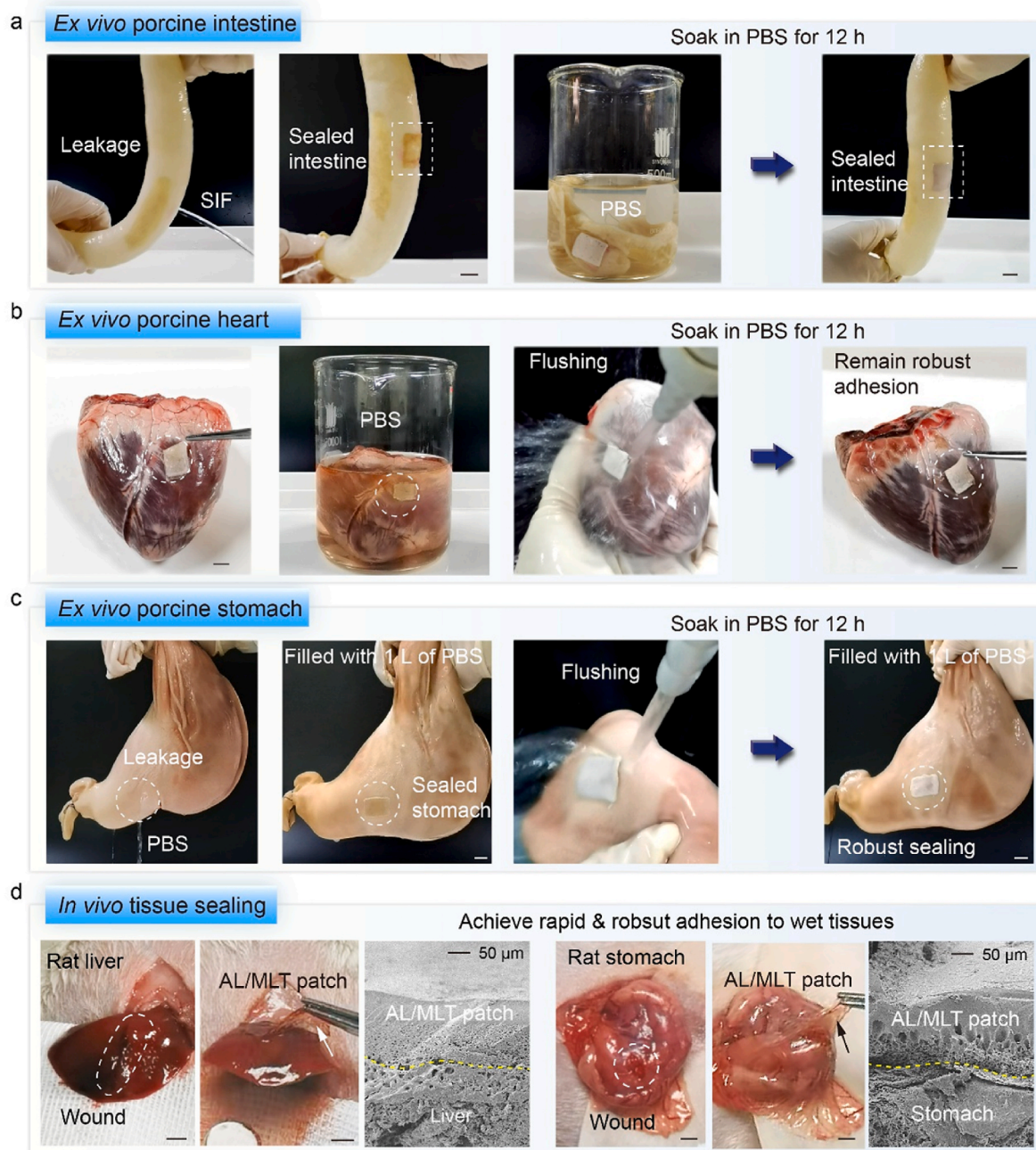


Fig. 4. Demonstration of the wound-sealing ability of the AL/MLT patch on *ex vivo* and *in vivo* organs. (a) *Ex vivo* wound sealing of porcine intestine (an incision of 1 cm) filled with PBS (pH = 7.2) before and after being immersed in PBS for 12 h. (b) Adhesion of AL/MLT patch on the surfaces of porcine heart before/after 12-h immersion in PBS and water flushing. (c) *Ex vivo* wound sealing of porcine stomach (an incision of 1 cm) filled with 1 L of PBS (pH = 7.2) before/after being immersed in PBS for 12 h. Scale bar: 1 cm. (d) Digital images and SEM images of an AL/MLT patch (thickness of 0.15 mm) adhered to the rat liver or stomach surface with a gentle press of 15 s, scale bar: 3 mm. The dotted yellow line delineates the adhesion interface between the AL/MLT patch and tissues. The AL/MLT patches hold a thickness of 0.4 mm when used to seal the porcine organs and 0.15 mm when used to seal the rat organs.

critical-sized gastric defect (a 4-mm perforation) on rats was carefully constructed. The sutureless wound sealing & healing of the defect and anti-postoperative adhesion capability enabled by the *Janus* AL/MLT patch (Fig. 5a) were evaluated. Treatments with surgical suturing and commercially available fibrin glue served as the controls.

During surgery, suturing proved to be time-consuming (over 5 min) and caused additional mechanical damage to gastric tissues due to needle piercing. Although the injectable fibrin gel was capable of gelation within 1 min to seal the gastric wound, it required a preoperative procedure with the assistance of a specific fluidic bicomponent mixer to prepare the gel precursor. In contrast, the ready-to-use AL/MLT patch (diameter: 12 mm) could firmly adhere to the tissue defect within 15 s of gentle pressing, enabling less blood loss and rapid wound sealing (Fig. 5b). At day 7 post-operation, the surgical site sealed either by suture or fibrin glue exhibited severe post-operative adhesion to the surrounding tissues/organs (e.g., liver and intestine). This is likely due to the leakage of gastric fluid/blood or the undesired adhesion of the homogeneous fibrin gel to surrounding tissues. In comparison, the AL layer of the AL/MLT patch enabled fluid-tight sealing to gastric defects, while the MLT layer of the AL/MLT patch showed a smooth surface without any tissue adhesion (Fig. 5c). H&E staining images further confirmed the significantly inhibited postoperative tissue adhesion enabled by the MLT layer (Fig. 5d). This could be attributed to the overall neutrally charged MLT hydrogel, which exhibited good resistance to cell adhesion (Fig. S15). Notably, the mucosal layer around the wound in the suturing and fibrin gel groups showed obvious interruptions (1.6 mm and 0.4 mm, Fig. 5d). In contrast, the AL/MLT hydrogel tightly adhered to the gastric surface without adhesion to surrounding tissues, completely bridging the perforation with regenerated seromuscular tissues and a well-integrated mucosa layer (Fig. 5d). Combined with *in vitro* wound sealing results (Fig. 3e), these data suggest that the AL/MLT adhesive could outperform the commercially available fibrin gel in achieving robust & stable tissue adhesion, as well as effective prevention of post-operative tissue adhesion.

Furthermore, the inflammation infiltration around the repaired gastric defect was assessed through immunofluorescence staining against TNF- α (a marker for pro-inflammatory cytokines). Fluorescence images showed a bright fluorescence intensity in the suture group, indicating the pro-inflammatory infiltration in the sutured tissues (Fig. 5e). Further quantitative analysis indicated a significant reduction in inflammatory infiltration in both fibrin gel and AL/MLT groups compared with the conventional suture treatment (Fig. 5e and h). Notably, no statistically significant difference was observed between the fibrin gel and AL/MLT groups. This could be attributed to their minimally invasive operation on tissues and good biocompatibility. To evaluate the effect of different treatments on neovascularization, the capillary density at the wound area was visualized by immunohistochemical staining for CD31 (a marker for endothelial cells and angiogenesis). Results revealed that the capillary density in the granulation tissue of the AL/MLT group was significantly higher than that in the fibrin gel group, indicating enhanced angiogenesis (as shown by green arrows, Fig. 5f) in the AL/MLT-treated gastric wound (Fig. 5h). Overall, these findings strongly suggest that the AL/MLT patch can enable robust & long-lasting adhesion for effective sealing and promote the gastric defect repairing, while significantly inhibiting postoperative tissue adhesion. The AL/MLT patch demonstrated here represents an early-stage tissue adhesive. Considering that healing gastric tissue may be mechanically weaker than healthy tissues in the early post-injury and more susceptible to reperforation [58], further in-depth investigations into the long-term sealing and repairing performance, stability, and biocompatibility of the AL/MLT patch for gastric perforation treatment will be required and are our plan. Nevertheless, preliminary experimental results indicate that the AL/MLT hydrogel patch can maintain stable adhesion during the initial healing process, capable of acting as a physical barrier to prevent fluid leakage.

3.4. *In vitro* antibacterial performance

Surgical site infections (SSIs) is one of the major clinical concerns regarding tissue repair, as they can amplify inflammatory responses and delay wound healing [59–62]. Despite the extremely sterile surgical conditions, SSIs can still occur due to the potential spread of bacteria from the patient's endogenous bacterial flora [4,60], especially in the gastrointestinal region [63,64]. The standard treatment for SSIs involves the administration of antibiotics. However, the overuse of these medications has contributed to the growing crisis of drug resistance [65].

As a natural cationic polymer, EPL can disrupt bacterial cell membranes through electrostatic interactions, exhibiting broad-spectrum antibacterial activity without contributing to drug resistance [46]. Within the AL/MLT patch, EPL is dynamically crosslinking with carboxyl polymers, allowing for partial release into the surrounding environment. After 9-h incubation, only a few visible bacterial colonies grew on agar plates of the AL, MLT, and AL/MLT groups as compared to that of the control group (Fig. 6a). Further quantitative analysis indicated that the effective bactericidal ability of the AL, MLT, and AL/MLT patches, with reductions of 97.3 %, 93.4 %, and 97.4 % against *S. aureus* (Figs. 6b) and 95.8 %, 99.8 %, and 98.2 % against *E. coli*, suggesting the broad-spectrum bactericidal activity of the AL/MLT patch, attributable to the EPL component in both hydrogels. Live/dead staining demonstrated that the majority of bacterial cells in the AL/MLT group were stained red, indicating cell death, while almost all bacteria in the control group remained alive (Fig. 6c). SEM imaging of *S. aureus* and *E. coli* cells demonstrated intact globular (*S. aureus*) or rod-like (*E. coli*) morphology in control groups. In vast contrast, both *S. aureus* and *E. coli* cells in the AL/MLT group exhibited deformed morphologies with cytoplasmic substances leakage (indicated by the yellow arrows, Fig. 6d). With the increasing risk of antimicrobial resistance (AMR), wound infections caused by drug-resistant bacteria (e.g., MRSA and *P. aeruginosa*) have become a major clinical concern [66,67]. To evaluate the antibacterial efficacy of the AL/MLT patch against drug-resistant bacteria, antibacterial assays were conducted on MRSA and *P. aeruginosa*. Results showed that the AL/MLT patch also demonstrated a significant bactericidal efficiency of 84.7 % against MRSA and 87.9 % against *P. aeruginosa* (Fig. 6e–h), further validating its broad-spectrum antibacterial activity. These findings strongly suggest that the *Janus* AL/MLT patch exhibits efficient & broad-spectrum antibacterial activity for preventing potential wound infections following tissue trauma.

3.5. *In vitro* biocompatibility, antioxidant ability, and *in vivo* degradation assay

Good biocompatibility is essential for the safe *in vivo* application of bio-adhesives. To preliminarily test the biocompatibility of the AL/MLT patch, the cytotoxicity and hemolytic assay were performed. The viabilities of L929 cells cultured in the AL, MLT, and AL/MLT-conditioned DMEM for 1, 3, and 5 days were comparable to that incubated in the regular DMEM (Fig. 7a and b), suggesting low cytotoxicity of the AL, MLT, and AL/MLT patches. Additionally, L929 cells in these groups also exhibited good proliferation as the culture time increased. Live/dead staining images showed that L929 cells grew well after co-incubation for 5 days, and almost no dead cells were observed. Hemolytic activity assay showed that the supernatant color in the AL/MLT group resembled that of the PBS group, exhibiting a pale pink hue without significant differences (Fig. 7d). The calculated hemolysis ratio of the AL/MLT patch was 1.7 %, well below the ASTM standard of 5 % [68,69], indicating good hemocompatibility (Fig. 7e).

Reactive oxygen species (ROS) are critical for cellular metabolism. However, excessive ROS can induce oxidative stress and abnormal inflammatory responses, thereby delaying the wound-healing process [70]. Developing functional bio-adhesives that can scavenge excessive ROS at the wound sites is an effective strategy to promote wound healing. To improve the antioxidant activity of the tissue patch, a small

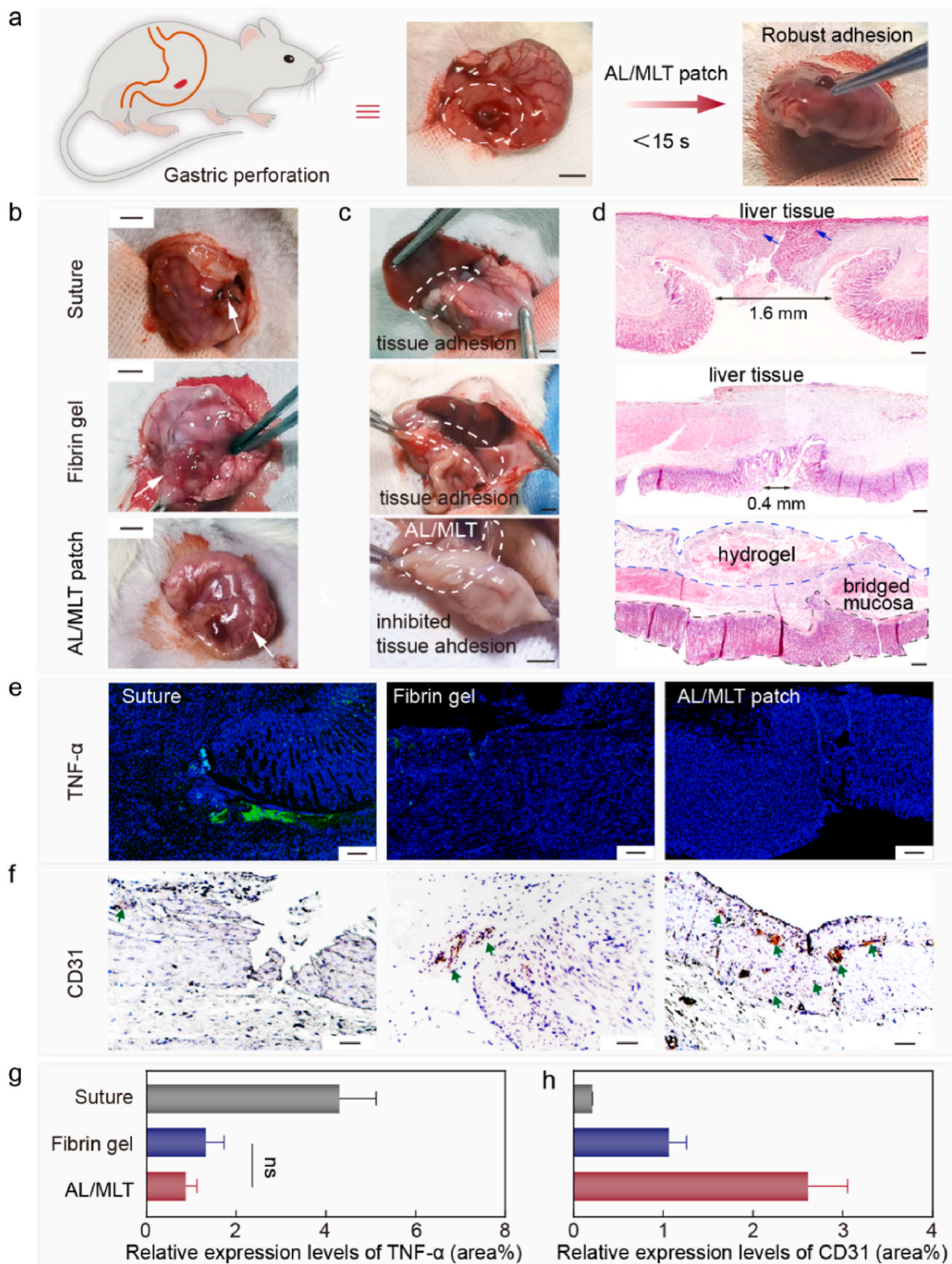


Fig. 5. Sealing and repairing of gastric tissue defects by the AL/MLT patch. (a) Schematic illustration and digital image of the gastric perforation. Scale bar: 8 mm. (b) Images of the surgical procedures performed to seal gastric defects by suture, fibrin glue, and AL/MLT patch, respectively. Scale bar: 4 mm. (c) Images at the surgical site with different treatments after 7-day operation. Scale bar: 4 mm. (d) H&E staining images of the gastric wound at day 7 post-operation. Scale bar: 200 μ m. Blue arrows indicate the liver tissues. (e) Images of immunofluorescence staining against TNF- α (indicated by the green fluorescence). Scale bar: 100 μ m. (f) Images of immunohistochemical staining against CD31 (indicated by green arrows). Scale bar: 50 μ m. Quantitative analysis of relative expression levels of (g) TNF- α and (h) CD31. Quantitative analysis ($n = 3$) of the immunofluorescence staining images for TNF- α was performed using Image J software. Quantitative analysis ($n = 3$) of the immunohistochemical (IHC) staining images for CD31 was performed using Image J software with the IHC Image Analysis Toolbox plugin. Pairwise comparisons are statistically significant (*, $p < 0.05$) unless denoted as “ns” as determined by one-way ANOVA multiple comparisons between multiple groups.

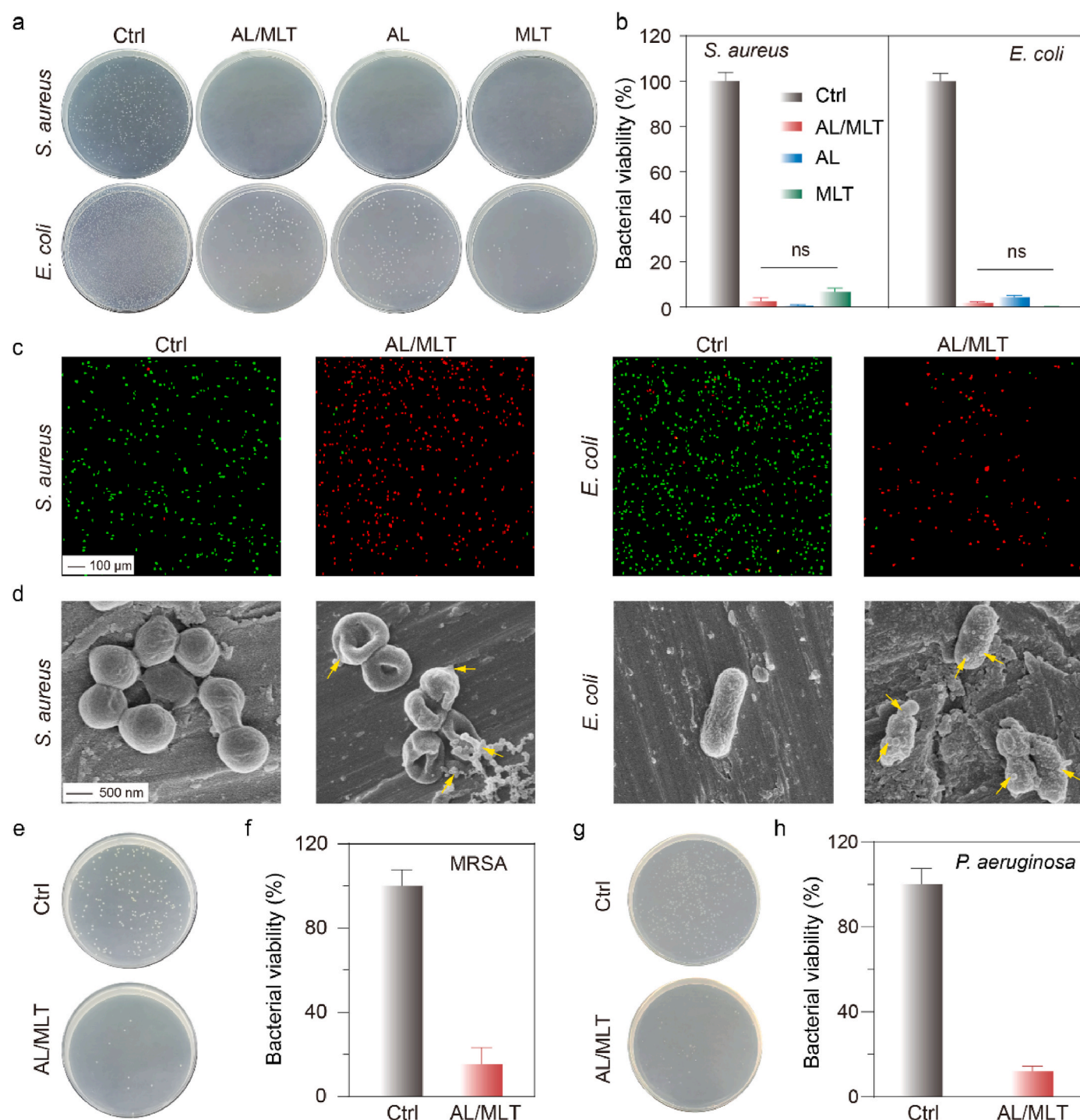


Fig. 6. *In vitro* antibacterial assay of the AL/MLT patch: (a) Images of *S. aureus* and *E. coli* colonies grew on agar plates after 9-h incubation with AL, MLT, and AL/MLT patches in PBS. Control group: bacteria cultured in PBS without samples. (b) Bacterial viability of *S. aureus* and *E. coli*. (c) CLSM and (d) SEM images of *S. aureus* and *E. coli* cells seeded on a titanium sheet after 9-h incubation with AL/MLT patches in PBS. The yellow arrows indicated the leakage site. Images of MRSA (e) and *P. aeruginosa* (g) colonies grew on the agar plate after 9-h incubation with the AL/MLT patch, and corresponding bacterial viability quantification of MRSA (f) and *P. aeruginosa* (h). Pairwise comparisons are statistically significant (*, $p < 0.05$) unless denoted as “ns” as determined by one-way ANOVA multiple comparisons between multiple groups or Student’s t-test for comparisons between two groups ($n = 3$).

amount of tannic acid was incorporated within the ML powder due to its excellent antioxidant capacity stemming from multiple phenolic hydroxyl groups [71]. After adding MLT powder to the DPPH· solution at 37 °C, a significantly reduced intensity of DPPH· (absorption at 517 nm) was detected, while no obvious decrease of DPPH· signal in ML powder and control groups (Fig. 7f and S16). When the incubation time was prolonged to 3 h, the reduction in the intensity of the DPPH· signal was

further increased from 68.7 % to 90.3 % (Fig. 7g), indicating a strong ability to eliminate surrounding ROS.

When exogenous H₂O₂ was introduced in the cell culture medium, bright green fluorescence in L-02 cells was observed in the positive control (+) and ML hydrogel groups (Fig. 7h and S17), indicating elevated intracellular ROS levels. In contrast, fluorescence intensity inside the L-02 cells cultured with MLT hydrogel was significantly

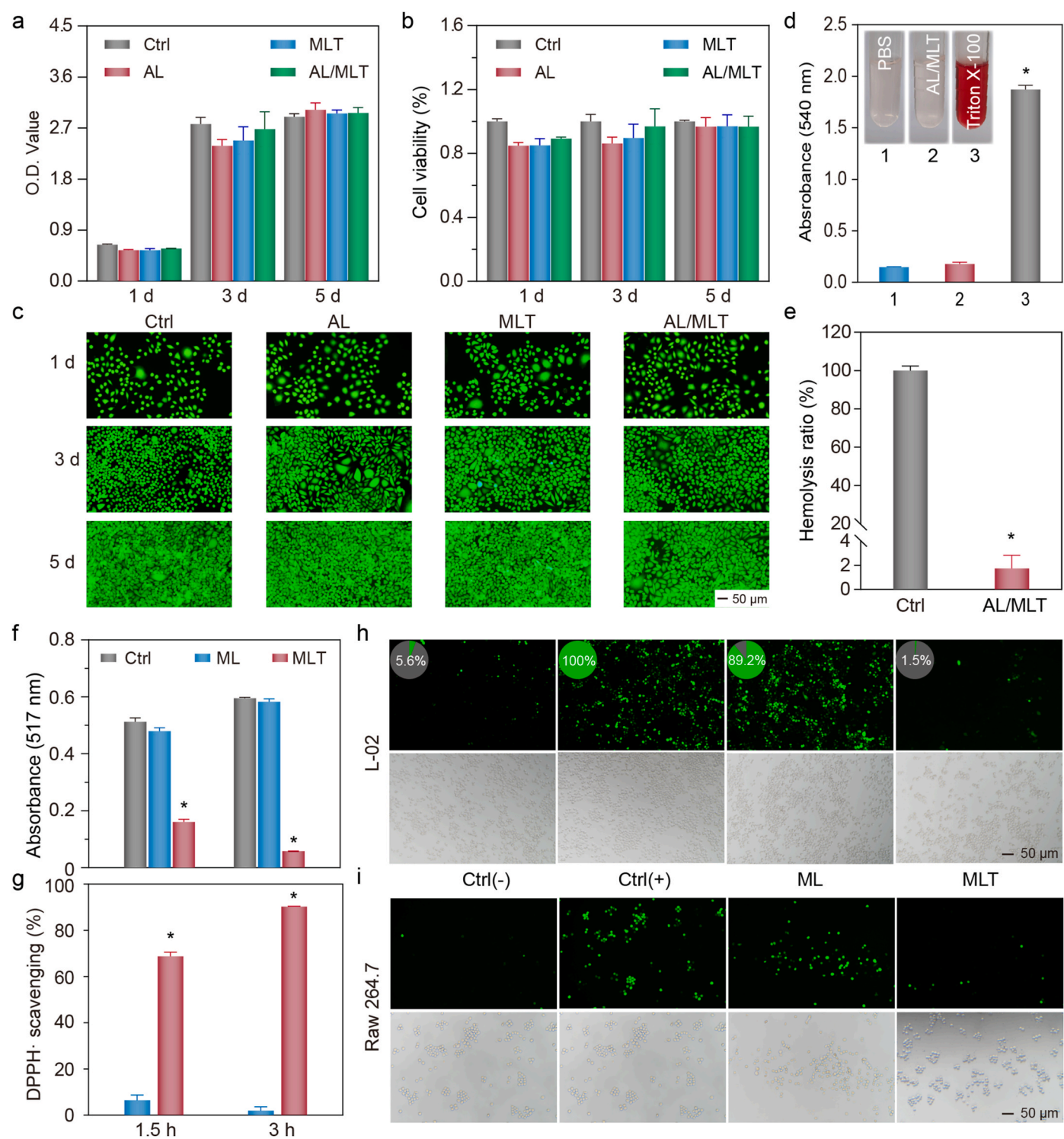


Fig. 7. *In vitro* biocompatibility and antioxidant ability. (a) *In vitro* proliferation abilities and (b) cell viabilities of L929 cells after incubation with the extracts of AL, MLT, and AL/MLT patches for 1, 3, and 5 days. (c) Fluorescence microscope images of live/dead L929 cells. (d) Absorbance at 540 nm of the supernatants in PBS, AL/MLT, and Triton \times 100 groups after 1-h incubation with rat red cells at 37 $^{\circ}$ C. (e) Hemolysis ratio of the AL/MLT patch. (f) Absorbance at 517 nm of the DPPH·-methanol solution after incubation with ML and MLT powders for 1.5 and 3 h at 37 $^{\circ}$ C, respectively. The DPPH·-methanol solution was set as the control group. (g) DPPH·-scavenging ratios of ML and MLT powders. Representative fluorescence images of intracellular ROS generation in (h) L-02 and (i) Raw.264.7 cells. The ctrl (-) group indicated the normal cells without H_2O_2 stimulation. Pairwise comparisons are statistically significant unless denoted as “ns” (not significant) as determined by Student’s t-test for comparisons between two groups and by one-way ANOVA multiple comparisons for the comparisons between multiple groups.

decreased to 1.5%, similar to that of L-02 cells without H_2O_2 stimulation (negative control). Similar results were observed on Raw264.7 cells (Fig. 7i). These findings suggest that incorporating a trace amount of tannic acid into the MLT hydrogel can efficiently endow additional

function/ability to the adhesive patch to scavenge the overproduced ROS, thereby preventing cells from oxidative stress.

Suitable biodegradability is essential for bioadhesives to match the wound-healing processes. Since the AL/MLT patch is a physically

crosslinked hydrogel with a biodegradable EPL component, the overall *in vivo* biodegradation of the AL/MLT patch was conducted with a subcutaneous implantation model on rats (Fig. 8a). After 2 weeks of implantation, bulk AL/MLT adhesive was clearly visible subcutaneously at the surgical site (Fig. 8b & S18). This preservation could be attributed to the robust physical crosslinking between carboxyl and amine groups in the physiological environment, which ensures effective and lasting wound sealing. Notably, the top MTL layer in the AL/MLT adhesive exhibited no adhesion to surrounding tissues within 2 weeks. This could be attributed to the good electroneutrality retention of the MLT hydrogel, as evidenced by the zeta potentials of the MLT hydrogel (Fig. S19) after immersion in PBS for 1, 7, and 14 days. As the implantation time extended to 6 weeks, the hydrogel appeared smaller (Fig. 8b). Remarkably, almost no visible hydrogel remained at the surgical site after 10 weeks (Fig. 8b). H&E histological images further confirmed the subcutaneous retention of a bulk hydrogel at 6 weeks (indicated by red dashed lines) and revealed only a small hydrogel fragment embedded in surrounding tissues at 10 weeks (Fig. 8c–e), suggesting that the majority of the AL/MLT hydrogel degrades within 10 weeks. In addition, H&E images verified no tissue adhesion at the MLT/tissue interface within 6

weeks (a clear gap between the MLT layer and top tissue, Fig. 8d), indicating that the MLT layer with the balanced charge that mimics the electroneutral nature of zwitterionic materials, could endow effective anti-tissue adhesion ability to the *Janus* tissue patch during the wound healing process (Fig. 8c and d).

4. Conclusion

In summary, we have introduced a new strategy to construct an adhesive/anti-adhesive *Janus* hydrogel bioadhesive without varied chemical design of the hydrogel layers. Based on pH adjustment of the similar polyelectrolyte complex, the bottom hydrogel layer (formed at an acidic pH) possesses massive $-\text{COOH}/-\text{NH}_3^+$ paired groups, resulting in a net positively charged structure. This configuration provides rapid & robust adhesion to diverse wet tissues. Conversely, the top hydrogel layer (formed at neutral pH) possessing massive $-\text{COOH}/-\text{NH}_2$ and $-\text{COO}^-/-\text{NH}_3^+$ groups, resulting in an overall electroneutral structure, endowed excellent anti-adhesive properties to the patch. The integrated AL/MLT patch effectively promotes wound sealing and healing, significantly inhibits post-operative tissue adhesion, and outperforms

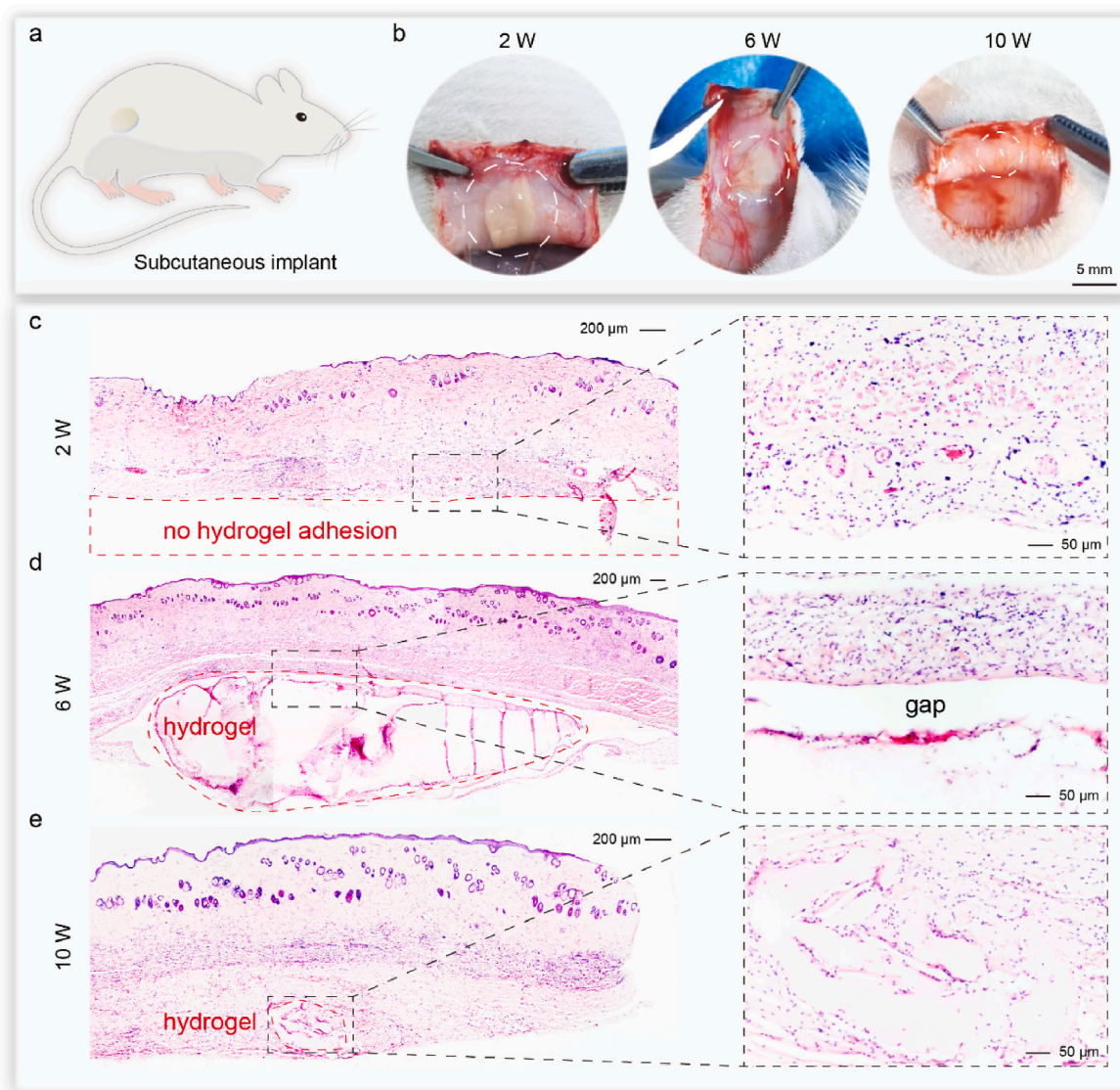


Fig. 8. *In vivo* biodegradability and anti-tissue adhesion assay: (a) Schematic illustration of the subcutaneous implantation of the AL/MLT patch on the rat's back skin. (b) *In situ* images of AL/MLT hydrogels after implantation for 2, 6, and 10 weeks. Representative H&E histological images around AL/MLT hydrogel (indicated by the red dashed lines) after subcutaneous implantation for (c) 2, (d) 6, and (e) 10 weeks.

commercially available fibrin gel in rat gastric defect models. In addition to its adhesive/anti-adhesive properties, the cationic EPL component endowed efficient broad-spectrum bactericidal activity to the patch. The AL/MLT patch is cytocompatible, blood-compatible, and biodegradable aligning with the natural healing process. Furthermore, incorporating a trace amount of tannic acid can enhance the ability of the patch adhesive to scavenge the overproduced ROS and prevent cells from oxidative stress, potentially making it especially suitable for sealing & healing chronic wounds.

The AL/MLT patch demonstrated in this article represents an early stage of a tissue adhesive that aims to introduce a strategy for engineering an adhesive/anti-adhesive *Janus* bioadhesive by switching the charge balance of the hydrogel layers with similar chemical compositions, and further in-depth investigations, such as long-term adverse effects of the degradation by-products, general application on other tissues/organs, and scale-up animal studies will be required. Nevertheless, these *in vitro* and *in vivo* findings have highlighted the advantages of the AL/MLT patch as tissue adhesives for internal wound closure and repair. The facile fabrication, easy customization in dimensions, ready-to-use operation, effective adhesion/anti-adhesion performances, good biocompatibility and biodegradability, and efficient antibacterial activities make the *Janus* patch an advanced tissue adhesive for non-invasive wound closure and tissue repair.

CRedit authorship contribution statement

Wan Peng: Writing – original draft, Visualization, Validation, Resources, Investigation, Formal analysis, Data curation. **Youjin Lai:** Writing – original draft, Methodology, Formal analysis, Data curation. **Yefeng Jiang:** Validation, Methodology, Formal analysis, Data curation. **Yang Zhang:** Writing – original draft, Methodology, Formal analysis, Data curation. **Zilin Kan:** Writing – original draft, Methodology, Formal analysis, Data curation. **Chuanhao Dai:** Writing – original draft, Visualization, Validation, Investigation, Formal analysis. **Jian Shen:** Writing – original draft, Visualization, Validation, Methodology, Investigation, Formal analysis. **Pingshen Liu:** Writing – review & editing, Supervision, Project administration, Investigation, Funding acquisition, Conceptualization.

Ethics approval and consent to participate

Related *in vivo* experimental procedures complied with ethical principles and conformed to the Animal Management Regulations of China and were approved by the Institutional Animal Care and Use Committee (IACUC) of Nanjing Normal University (Approval Number: IACUC-20230914).

Declaration of competing interest

The authors declare that they have no known competing financial interests or personal relationships that could have appeared to influence the work reported in this paper.

Acknowledgments

Authors thank the grant supports from the Six Talent Peaks Project in Jiangsu Province (SWYY-060), Changzhou City Major Technology Demand "Unveiling and Leading" Science and Technology Research Project (S11090B42215), and the Postdoctoral Fellowship Program of CPSF under Grant Number GZC20231142.

Appendix A. Supplementary data

Supplementary data to this article can be found online at <https://doi.org/10.1016/j.bioactmat.2025.06.006>.

References

- [1] G.P. Dobson, Trauma of major surgery: a global problem that is not going away, *Int. J. Surg.* 81 (2020) 47–54, <https://doi.org/10.1016/j.ijso.2020.07.017>.
- [2] A.S. Richard, R.S. Verma, Bioactive nano yarns as surgical sutures for wound healing, *Mater. Sci. Eng. C* 128 (2021) 112334, <https://doi.org/10.1016/j.msec.2021.112334>.
- [3] E.S. Saber, A.M. Ibrahim, F.M. Benjamine, Effects and results of omentopexy during laparoscopic sleeve gastrectomy on possible post operative bleeding and/or leakage, *QJM: Int. J. Med.* 113 (Supplement_1) (2020) 193, <https://doi.org/10.1093/qjmed/hcaa050.015>.
- [4] M. Renko, N. Paalanne, T. Tapiainen, M. Hinkkainen, T. Pokka, S. Kinnula, J. J. Sinikumpu, M. Uhari, W. Serlo, Triclosan-containing sutures versus ordinary sutures for reducing surgical site infections in children: a double-blind, randomised controlled trial, *Lancet Infect. Dis.* 17 (1) (2017) 50–57, [https://doi.org/10.1016/S1473-3099\(16\)30373-5](https://doi.org/10.1016/S1473-3099(16)30373-5).
- [5] M. Tummalapalli, S. Anjum, S. Kumari, B. Gupta, Antimicrobial surgical sutures: recent developments and strategies, *Polym. Rev.* 56 (4) (2016) 607–630, <https://doi.org/10.1080/15583724.2015.1119163>.
- [6] M. Puthia, J. Petrlova, G. Petruk, M. Butrym, F. Samsudin, M.A. Andersson, A. C. Stromdahl, S. Wasserstrom, E. Hartman, S. Kjellstrom, L. Caselli, O. Klementieva, P.J. Bond, M. Malmsten, D.B. Raina, A. Schmidtchen, Bioactive suture with added innate defense functionality for the reduction of bacterial infection and inflammation, *Adv. Healthcare Mater.* 12 (31) (2023) e2300987, <https://doi.org/10.1002/adhm.202300987>.
- [7] Z. Wan, J. He, Y. Yang, T. Chong, J. Wang, B. Guo, L. Xue, Injectable adhesive self-healing biocompatible hydrogel for haemostasis, wound healing, and postoperative tissue adhesion prevention in nephron-sparing surgery, *Acta Biomater.* 152 (2022) 157–170, <https://doi.org/10.1016/j.actbio.2022.09.006>.
- [8] G.M. Taboada, K. Yang, M.J.N. Pereira, S.S. Liu, Y. Hu, J.M. Karp, N. Artzi, Y. Lee, Overcoming the translational barriers of tissue adhesives, *Nat. Rev. Mater.* 5 (4) (2020) 310–329, <https://doi.org/10.1038/s41578-019-0171-7>.
- [9] Z. Bao, M. Gao, Y. Sun, R. Nian, M. Xian, The recent progress of tissue adhesives in design strategies, adhesive mechanism and applications, *Mater. Sci. Eng. C* 111 (2020) 110796, <https://doi.org/10.1016/j.msec.2020.110796>.
- [10] W.D. Spotnitz, Fibrin sealant: the only approved hemostat, sealant, and adhesive-a laboratory and clinical perspective, *ISRN Surg* 2014 (2014) 203943, <https://doi.org/10.1155/2014/203943>.
- [11] J. Wang, X. Tian, W. Zhang, X. Dong, Z. Wang, S. Wang, Y. Liang, W. Wang, L. Xu, Y. Li, A cyanoacrylate/triethyl citrate/nanosilica-based closure glue with wet-adhesion capability for treatment of superficial varicose veins, *J. Mater. Chem. B* 11 (20) (2023) 4548–4555, <https://doi.org/10.1039/d3tb00408b>.
- [12] C.J. Hannan, D. Nolan, P. Corr, M. Amoo, D. Murray, S. Looby, M. Javadpour, Sinonasal outcomes associated with the use of BioGlue(R) in endoscopic transphenoidal pituitary surgery, *Neurosurg. Rev.* 45 (3) (2022) 2249–2256, <https://doi.org/10.1007/s10143-021-01723-x>.
- [13] N. Shimony, A. Shagan, B.H. Eylon, A. Nyska, A. Gross, B. Mizrahi, Liquid copolymers as biodegradable surgical sealant, *Adv. Healthcare Mater.* 10 (19) (2021) 2100803, <https://doi.org/10.1002/adhm.202100803>.
- [14] Y. Zhao, S. Song, X. Ren, J. Zhang, Q. Lin, Y. Zhao, Supramolecular adhesive hydrogels for tissue engineering applications, *Chem. Rev.* 122 (6) (2022) 5604–5640, <https://doi.org/10.1021/acs.chemrev.1c00815>.
- [15] C. Cui, W. Liu, Recent advances in wet adhesives: adhesion mechanism, design principle and applications, *Prog. Mater. Sci.* 116 (2021) 101388, <https://doi.org/10.1016/j.progpolymsci.2021.101388>.
- [16] H.X. Yujie Hua, Litao Jia, Jinzhong Zhao, Dandan Zhao, Xiaoyu Yan, Yiqing Zhang, Shengjian Tang, Guangdong Zhou, Linyong Zhu, Qiuning Lin, Ultrafast, tough, and adhesive hydrogel based on hybrid photocrosslinking for articular cartilage repair in water-filled arthroscopy, *Sci. Adv.* 7 (35) (2021) eabg0628, <https://doi.org/10.1126/sciadv.abg0628>.
- [17] Z. Wang, X. Gu, B. Li, J. Li, F. Wang, J. Sun, H. Zhang, K. Liu, W. Guo, Molecularly engineered protein glues with superior adhesion performance, *Adv. Mater.* 34 (41) (2022) e2204590, <https://doi.org/10.1002/adma.202204590>.
- [18] J. He, Z. Zhang, Y. Yang, F. Ren, J. Li, S. Zhu, F. Ma, R. Wu, Y. Lv, G. He, B. Guo, D. Chu, Injectable self-healing adhesive pH-responsive hydrogels accelerate gastric hemostasis and wound healing, *Nano-Micro Lett.* 13 (1) (2021) 80, <https://doi.org/10.1007/s40820-020-00585-0>.
- [19] Z.Z. Hui Ren, Xueliang Cheng, Zheng Zou, Xuesi Chen, Chaoliang He, Injectable, self-healing hydrogel adhesives with firm tissue adhesion and on-demand biodegradation for sutureless wound closure, *Sci. Adv.* 9 (2023) eadh4327, <https://doi.org/10.1126/sciadv.adh4327>.
- [20] X. Zhao, Y. Huang, Z. Li, J. Chen, J. Luo, L. Bai, H. Huang, E. Cao, Z. Yin, Y. Han, B. Guo, Injectable self-expanding/self-propelling hydrogel adhesive with procoagulant activity and rapid gelation for lethal massive hemorrhage management, *Adv. Mater.* 36 (15) (2024) 2308701, <https://doi.org/10.1002/adma.202308701>.
- [21] X. Chen, J. Zhang, G. Chen, Y. Xue, J. Zhang, X. Liang, I.M. Lei, J. Lin, B.B. Xu, J. Liu, Hydrogel bioadhesives with extreme acid-tolerance for gastric perforation repairing, *Adv. Funct. Mater.* 32 (29) (2022) 2202285, <https://doi.org/10.1002/adfm.202202285>.
- [22] K. Zhang, X. Chen, Y. Xue, J. Lin, X. Liang, J. Zhang, J. Zhang, G. Chen, C. Cai, J. Liu, Tough hydrogel bioadhesives for sutureless wound sealing, hemostasis and biointerfaces, *Adv. Funct. Mater.* 32 (15) (2021) 2111465, <https://doi.org/10.1002/adfm.202111465>.

- [23] H. Yuk, C.E. Varela, C.S. Nabzdyk, X. Mao, R.F. Padera, E.T. Roche, X. Zhao, Dry double-sided tape for adhesion of wet tissues and devices, *Nature* 575 (2019) 169–174, <https://doi.org/10.1038/s41586-019-1710-5>.
- [24] Jingjing Wu, Hyunwoo Yuk, L.S. Tiffany, Chuan Fei Guo, Leigh G. Griffiths, Christoph S. Nabzdyk, X. Zhao, An off-the-shelf bioadhesive patch for sutureless repair of gastrointestinal defects, *Sci. Transl. Med.* 14 (2022), <https://doi.org/10.1126/scitranslmed.abb2857> eabh2857.
- [25] B. Xue, J. Gu, L. Li, W. Yu, S. Yin, M. Qin, Q. Jiang, W. Wang, Y. Cao, Hydrogel tapes for fault-tolerant strong wet adhesion, *Nat. Commun.* 12 (1) (2021) 7156, <https://doi.org/10.1038/s41467-021-27529-5>.
- [26] H. An, M. Zhang, Z. Huang, Y. Xu, S. Ji, Z. Gu, P. Zhang, Y. Wen, Hydrophobic Cross-linked chains regulate high wet tissue adhesion hydrogel with toughness, anti-hydration for dynamic tissue repair, *Adv. Mater.* 36 (8) (2023) 2310164, <https://doi.org/10.1002/adma.202310164>.
- [27] P. Ma, W. Liang, R. Huang, B. Zheng, K. Feng, W. He, Z. Huang, H. Shen, H. Wang, D. Wu, Super-structured wet-adhesive hydrogel with ultrahigh swelling, ultrahigh burst pressure tolerance, and anti-postoperative adhesion properties for tissue adhesion, *Adv. Mater.* 36 (11) (2023) 2305400, <https://doi.org/10.1002/adma.202305400>.
- [28] W. Yang, C. Xuan, X. Liu, Q. Zhang, K. Wu, L. Bian, X. Shi, A sandwiched patch toward leakage-free and anti-postoperative tissue adhesion sealing of intestinal injuries, *Bioact. Mater.* 24 (2023) 112–123, <https://doi.org/10.1016/j.bioactmat.2022.12.003>.
- [29] Yu Wang, Guopu Chen, Lingyu Sun, Xiaoxuan Zhang, Yuanjin Zhao, Bio-inspired structural color patch with anisotropic surface adhesion, *Sci. Adv.* 6 (4) (2020), <https://doi.org/10.1126/sciadv.aax8258> eaax8258.
- [30] P.C. Shanto, M.A.A. Fahad, H.I. Jung, M. Park, H. Kim, S.H. Bae, B.-T. Lee, Multi-functional dual-layer nanofibrous membrane for prevention of postoperative pancreatic leakage, *Biomaterials* 307 (2024) 122508, <https://doi.org/10.1016/j.biomaterials.2024.122508>.
- [31] Y. He, Q. Li, P. Chen, Q. Duan, J. Zhan, X. Cai, L. Wang, H. Hou, X. Qiu, A smart adhesive Janus hydrogel for non-invasive cardiac repair and tissue adhesion prevention, *Nat. Commun.* 13 (1) (2022) 7666, <https://doi.org/10.1038/s41467-022-35437-5>.
- [32] K. Chen, C. Liu, J. Huang, L. Che, Y. Yuan, C. Liu, A conformable and tough janus adhesive patch with limited 1d swelling behavior for internal bioadhesion, *Adv. Funct. Mater.* (2023) 2303836, <https://doi.org/10.1002/adfm.202303836>.
- [33] Y. Lv, F. Cai, X. Zhao, X. Zhu, F. Wei, Y. Zheng, X. Shi, J. Yang, Bioinspired microstructured janus bioadhesive for the prevention of abdominal and intrauterine adhesions, *Adv. Funct. Mater.* 34 (21) (2024) 2314402, <https://doi.org/10.1002/adfm.202314402>.
- [34] J. Yu, Y. Qin, Y. Yang, X. Zhao, Z. Zhang, Q. Zhang, Y. Su, Y. Zhang, Y. Cheng, Robust hydrogel adhesives for emergency rescue and gastric perforation repair, *Bioact. Mater.* 19 (2023) 703–716, <https://doi.org/10.1016/j.bioactmat.2022.05.010>.
- [35] L. Sun, J. Zhou, J. Lai, X. Zheng, H. Wang, B. Lu, R. Huang, L.M. Zhang, Novel natural polymer-based hydrogel patches with Janus asymmetric-adhesion for emergency hemostasis and wound healing, *Adv. Funct. Mater.* 34 (36) (2024) 2401030, <https://doi.org/10.1002/adfm.202401030>.
- [36] C. Cui, T. Wu, X. Chen, Y. Liu, Y. Li, Z. Xu, C. Fan, W. Liu, A Janus hydrogel wet adhesive for internal tissue repair and anti-postoperative adhesion, *Adv. Funct. Mater.* 30 (49) (2020) 2005689, <https://doi.org/10.1002/adfm.202005689>.
- [37] W. Peng, C. Liu, Y. Lai, Y. Wang, P. Liu, J. Shen, An adhesive/anti-adhesive Janus tissue patch for efficient closure of bleeding tissue with inhibited postoperative adhesion, *Adv. Sci.* 10 (21) (2023) e2301427, <https://doi.org/10.1002/advs.202301427>.
- [38] S.J. Wu, H. Yuk, J. Wu, C.S. Nabzdyk, X. Zhao, A multifunctional origami patch for minimally invasive tissue sealing, *Adv. Mater.* 33 (11) (2021) e2007667, <https://doi.org/10.1002/adma.202007667>.
- [39] W. Peng, Y. Lai, J. Fan, C. Dai, J. Shen, P. Liu, Simple component self-gelling powders as multifunctional tissue adhesives for sutureless wound healing, *Chem. Eng. J.* 495 (2024) 153514, <https://doi.org/10.1016/j.cej.2024.153514>.
- [40] W. Peng, P. Liu, X. Zhang, J. Peng, Y. Gu, X. Dong, Z. Ma, P. Liu, J. Shen, Multi-functional zwitterionic coating for silicone-based biomedical devices, *Chem. Eng. J.* 398 (2020) 125663, <https://doi.org/10.1016/j.cej.2020.125663>.
- [41] X. Dong, W. Peng, J. Sun, Y. Li, B. Fan, Y. Dong, D. Gan, W. Zhang, P. Liu, J. Shen, Zwitterionic/phosphonate copolymer coatings endow excellent antifouling properties and robust re-mineralization ability of dentine substrates, *J. Mater. Chem. B* 10 (31) (2022) 5976–5988, <https://doi.org/10.1039/d2tb00750a>.
- [42] W. Peng, B. Fan, Y. Li, Y. Dong, W. Qian, X. Ji, D. Gan, P. Liu, J. Shen, Layer-by-layer construction of zwitterionic/biuguanide polymers on silicone rubber as an antifouling and bactericidal coating, *J. Mater. Chem. B* 10 (39) (2022) 8013–8023, <https://doi.org/10.1039/d2tb01671k>.
- [43] A. Erfani, J. Seaberg, C.P. Aichele, J.D. Ramsey, Interactions between biomolecules and zwitterionic moieties: a review, *Biomacromolecules* 21 (7) (2020) 2557–2573, <https://doi.org/10.1021/acs.biomac.0c00497>.
- [44] A. Banerjee, A. Ghosh, B. Saha, P. Bhadury, P. De, Surface charge-switchable antifouling block copolymer with bacteriostatic properties, *Langmuir* 40 (10) (2024) 5314–5325, <https://doi.org/10.1021/acs.langmuir.3c03771>.
- [45] J. Li, A.D. Celiz, J. Yang, Q. Yang, Tough adhesives for diverse wet surfaces, *Sci. Technol. Humanit.* 357 (6349) (2017) 378–381, <https://doi.org/10.1126/science.aah6362>.
- [46] N.A. Patil, B. Kandasubramanian, Functionalized polylysine biomaterials for advanced medical applications: a review, *Eur. Polym. J.* 146 (2021) 110248, <https://doi.org/10.1016/j.eurpolymj.2020.110248>.
- [47] P. Wan, Y. Wang, W. Guo, Z. Song, S. Zhang, H. Wu, W. Yan, M. Deng, C. Xiao, Low-molecular-weight polylysines with excellent antibacterial properties and low hemolysis, *ACS Biomater. Sci. Eng.* 8 (2) (2022) 903–911, <https://doi.org/10.1021/acsbomaterials.1c01527>.
- [48] W. Han, C. Chen, K. Yang, H. Wang, H. Xia, Y. Zhao, Y. Teng, G. Feng, Y.M. Chen, Hyaluronic acid and chitosan-based injectable and self-healing hydrogel with inherent antibacterial and antioxidant bioactivities, *Int. J. Biol. Macromol.* 227 (2023) 373–383, <https://doi.org/10.1016/j.ijbiomac.2022.12.037>.
- [49] Z. Guo, W. Xie, J. Lu, X. Guo, J. Xu, W. Xu, Y. Chi, N. Takuya, H. Wu, L. Zhao, Tannic acid-based metal phenolic networks for bio-applications: a review, *J. Mater. Chem. B* 9 (20) (2021) 4098–4110, <https://doi.org/10.1039/d1tb00383f>.
- [50] Y. Li, Y. Miao, L. Yang, Y. Zhao, K. Wu, Z. Lu, Z. Hu, J. Guo, Recent advances in the development and antimicrobial applications of metal-phenolic networks, *Adv. Sci.* 9 (27) (2022) e2202684, <https://doi.org/10.1002/advs.202202684>.
- [51] G. Pan, F. Li, S. He, W. Li, Q. Wu, J. He, R. Ruan, Z. Xiao, J. Zhang, H. Yang, Mussel- and barnacle cement protein-inspired dual-bionic bioadhesive with repeatable wet-tissue adhesion, multimodal self-healing, and antibacterial capability for nonpressing hemostasis and promoted wound healing, *Adv. Funct. Mater.* 32 (25) (2022) 2200908, <https://doi.org/10.1002/adfm.202200908>.
- [52] Y.Z. Jiamin Zhang, Jiayin Song, Jing Yang, Chao Pan, Xu Tong, Lei Zhang, Novel balanced charged alginate/PEI polyelectrolyte hydrogel that resists foreign-body reaction, *ACS Appl. Mater. Interfaces* 10 (8) (2018) 6879–6886, <https://doi.org/10.1021/acsmi.7b17670>.
- [53] T.L. Sun, T. Kurokawa, S. Kuroda, A.B. Ihsan, T. Akasaki, K. Sato, M.A. Haque, T. Nakajima, J.P. Gong, Physical hydrogels composed of polyampholytes demonstrate high toughness and viscoelasticity, *Nat. Mater.* 12 (10) (2013) 932–937, <https://doi.org/10.1038/nmat3713>.
- [54] Q. Li, C. Wen, J. Yang, X. Zhou, Y. Zhu, J. Zheng, G. Cheng, J. Bai, T. Xu, J. Ji, S. Jiang, L. Zhang, P. Zhang, Zwitterionic biomaterials, *Chem. Rev.* 122 (23) (2022) 17073–17154, <https://doi.org/10.1021/acs.chemrev.2c00344>.
- [55] C. Ghobril, M.W. Grinstaff, The chemistry and engineering of polymeric hydrogel adhesives for wound closure: a tutorial, *Chem. Soc. Rev.* 44 (7) (2015) 1820–1835, <https://doi.org/10.1039/c4cs00332b>.
- [56] H. Wang, X. Yi, T. Liu, J. Liu, Q. Wu, Y. Ding, Z. Liu, Q. Wang, An integrally formed Janus hydrogel for robust wet-tissue adhesive and anti-postoperative adhesion, *Adv. Mater.* 35 (23) (2023) e2300394, <https://doi.org/10.1002/adma.202300394>.
- [57] D. Jolliffe, Practical gastric physiology, *BJA Education* 9 (6) (2009) 173–177, <http://ceacup.oxfordjournals.org>.
- [58] X.X. Xin Peng, Xiayi Xu, Xuefeng Yang, Boguang Yang, Pengchao Zhao, Weihua Yuan, Philip Wai Yan Chiu, Liming Bian, Ultrafast self-gelling powder mediates robust wet adhesion to promote healing of gastrointestinal perforations, *Sci. Adv.* 7 (23) (2021) eabe8739, <https://doi.org/10.1126/sciadv.abe8739>.
- [59] Z. Wang, J. Chen, P. Wang, Z. Jie, W. Jin, G. Wang, J. Li, J. Ren, Surgical site infection after gastrointestinal surgery in China: a multicenter prospective study, *J. Surg. Res.* 240 (2019) 206–218, <https://doi.org/10.1016/j.jss.2019.03.017>.
- [60] J.L. Seidelman, C.R. Mantyh, D.J. Anderson, Surgical site infection prevention: a review, *JAMA* 329 (3) (2023) 244–252, <https://doi.org/10.1001/jama.2022.24075>.
- [61] B. Allegranzi, A.M. Aiken, N. Zeynep Kubilay, P. Nthumba, J. Barasa, G. Okumu, R. Mugarua, A. Elobu, J. Jombwe, M. Maimbo, J. Musowoya, A. Gayet-Ageron, S. M. Berenholtz, A multimodal infection control and patient safety intervention to reduce surgical site infections in Africa: a multicentre, before-after, cohort study, *Lancet Infect. Dis.* 18 (5) (2018) 507–515, [https://doi.org/10.1016/S1473-3099\(18\)30107-5](https://doi.org/10.1016/S1473-3099(18)30107-5).
- [62] X.Q. Xuezhe Liu, Linxia Nie, Bikun Zhou, Pengzhen Bu, Li Yang, Xinwen Xue, Bo Tang, Qian Feng, Kaiyong Cai, Nonswelling hydrogel patch with tissue-mimetic mechanical characteristics remodeling in vivo microenvironment for effective adhesion prevention, *ACS Nano* 18 (27) (2024) 17651–17671, <https://doi.org/10.1021/acsnano.4c02321>.
- [63] C. GlobalSurg, Surgical site infection after gastrointestinal surgery in high-income, middle-income, and low-income countries: a prospective, international, multicentre cohort study, *Lancet Infect. Dis.* 18 (5) (2018) 516–525, [https://doi.org/10.1016/S1473-3099\(18\)30101-4](https://doi.org/10.1016/S1473-3099(18)30101-4).
- [64] H. Thomas, Describing the global burden of infection after gastrointestinal surgery, *Nat. Rev. Gastroenterol. Hepatol.* 15 (4) (2018) 190, <https://doi.org/10.1038/nrgastro.2018.22>.
- [65] S. Baker, N. Thomson, F.X. Weill, K.E. Holt, Genomic insights into the emergence and spread of antimicrobial-resistant bacterial pathogens, *Sci. Technol. Humanit.* 360 (6390) (2018) 733–738, <https://doi.org/10.1126/science.aar3777>.
- [66] A. Panzures, 222-nm UVC light as a skin-safe solution to antimicrobial resistance in acute hospital settings with a particular focus on methicillin-resistant *Staphylococcus aureus* and surgical site infections: a review, *J. Appl. Microbiol.* 134 (3) (2023) 1–15, <https://doi.org/10.1093/jambio/ixad046>.
- [67] K.W. Abimbola Feyisara Adedegi-Olulana, Lucia Lafage, aia Pasquina-Lemonche, Mariana Tinajero-Trejo, Joshua A.F. Sutton, Bohdan Bilyk, Sophie E. Irving, Callum J. Portman Ross, Oliver J. Meacock, Sam A. Randerson, Ewan Beattie, David S. Owen, James Florence, William M. Durham, William M. Durham, Rebecca M. Corrigan, Jeffrey Green, Jamie K. Hobbs, Simon J. Foster, Two codendent routes lead to high-level MRSA, *Sci. Technol. Humanit.* 386 (2024) 573–580, <https://doi.org/10.1126/science.adn1369>.
- [68] L. Teng, Z. Shao, Q. Bai, X. Zhang, Y.S. He, J. Lu, D. Zou, C. Feng, C.M. Dong, Biomimetic glycopolymer hydrogels with tunable adhesion and microporous structure for fast hemostasis and highly efficient wound healing, *Adv. Funct. Mater.* 31 (43) (2021) 2105628, <https://doi.org/10.1002/adfm.202105628>.
- [69] N. Golafshan, R. Rezahasani, M. Tarkesh Esfahani, M. Kharaziha, S.N. Khorasani, Nanohybrid hydrogels of laponite: PVA-Alginate as a potential wound healing

- material, *Carbohydr. Polym.* 176 (2017) 392–401, <https://doi.org/10.1016/j.carbpol.2017.08.070>.
- [70] Y. Qian, Y. Zheng, J. Jin, X. Wu, K. Xu, M. Dai, Q. Niu, H. Zheng, X. He, J. Shen, Immunoregulation in diabetic wound repair with a photoenhanced glycyrrhizic acid hydrogel scaffold, *Adv. Mater.* 34 (29) (2022) e2200521, <https://doi.org/10.1002/adma.202200521>.
- [71] K. Wu, X. Wu, J. Guo, Y. Jiao, C. Zhou, Facile polyphenol-Europium assembly enabled functional poly(L-Lactic Acid) nanofiber mats with enhanced antioxidation and angiogenesis for accelerated wound healing, *Adv. Healthcare Mater.* 10 (19) (2021) e2100793, <https://doi.org/10.1002/adhm.202100793>.